ISSN 2693-0935

Ancient TL

Institute of Earth Surface Dynamics, University of Lausanne, 1015 Lausanne, Switzerland
http://ancienttl.org

December 2024, Volume 42, No. 2

Ancient TL

Started by the late David Zimmerman in 1977

Ancient TL

Editorial

Christoph Schmidt*
Institute of Earth Surface Dynamics, University of Lausanne, Quartier UNIL-Mouline,
Bâtiment Géopolis, 1015 Lausanne, Switzerland

*Corresponding Author: christoph.schmidt@unil.ch

Recently, the editing and production of Ancient TL transitioned from Greenville, North Carolina, USA, to Lausanne, Switzerland. I would like to take this opportunity to extend my sincere gratitude to all the previous Editors for their invaluable work and dedication over the years, which has been essential to the success of our community. As the new Editor of Ancient TL, I am delighted to announce a series of changes designed to enhance the journal's visibility, accessibility, and relevance within the luminescence and ESR research community. These changes, detailed below, will take effect from 1 January 2025.

To support these advancements, I am pleased to introduce a new Editorial Board, comprised of experts from around the world, reflecting diversity in terms of geographical affiliation, career stages, and gender (Figs. 1 and 2). This team will play a crucial role in guiding the journal's strategic direction and maintaining the quality standards of Ancient TL. We are also grateful for the continued support of the new Advisory Board, which includes former Editors and the head of the steering committee of the International Luminescence and Electron Spin Resonance Dating Association (ILEDA). Their experience will be instrumental in navigating complex editorial matters and ensuring adherence to the highest ethical standards.

Ancient TL has a longstanding tradition of publishing papers of practical relevance for luminescence and ESR dating techniques. To reflect the progression of our field, we are broadening the journal's scope to encompass a wider range of topics. This includes all methods for quantifying environmental dose rates, software and code for data processing, and applications of luminescence and ESR beyond dating, such as determining rates of geological processes, rock thermal histories, provenance, or for characterisation purposes. We also welcome contributions on interlaboratory comparisons, standardisation procedures, failed experiments and observations that are yet difficult to explain. We believe that publishing those results fills a gap left by other journals and stimulates discussion in the community.

Furthermore, we recognise the importance of an objective and thorough peer-review process. To this end, we are moving to a single-blind review system where authors are asked to suggest potential reviewers from our new Editorial Board or also from the broader research community, depending on the topic's requirements. While the final selection of reviewers rests with the handling editor, this adapted system ensures a fair and rigorous evaluation of the submitted works.

We are also introducing refined article formats to cater to the diverse needs of our authors. These include:

- Research Article (up to 10,000 words, 2 peer-reviews)
- Short Communication (up to 4,000 words, 1 peer-review)
- Spotlight review (invited, up to 5,000 words, 1 peer-review)
- Letter to the Editor, including comments on previous papers published in Ancient TL (1 peer-review)
- Thesis Abstract
- Corrigendum

This range of formats provides authors with more flexible options for presenting their research findings and engaging in scholarly dialogue.

In line with the growing emphasis on open science, Ancient TL will continue to publish diamond open access, henceforth using the SOAP2 platform which is based on Open Journal Systems. This platform offers a comprehensive editorial workflow and promotes transparency and efficiency throughout the publication process. With the transition to SOAP2, all Ancient TL articles, including past publications, will be assigned a Digital Object Identifier (DOI) and registered with CrossRef. The journal policies on publication ethics, data availability, and conflict of interest have been updated to ensure the integrity and credibility of the research published in Ancient TL.

We are confident that these changes will attract a wider range of submissions, including from early-career researchers, foster greater discussion within the research community and enhance the visibility and impact of the

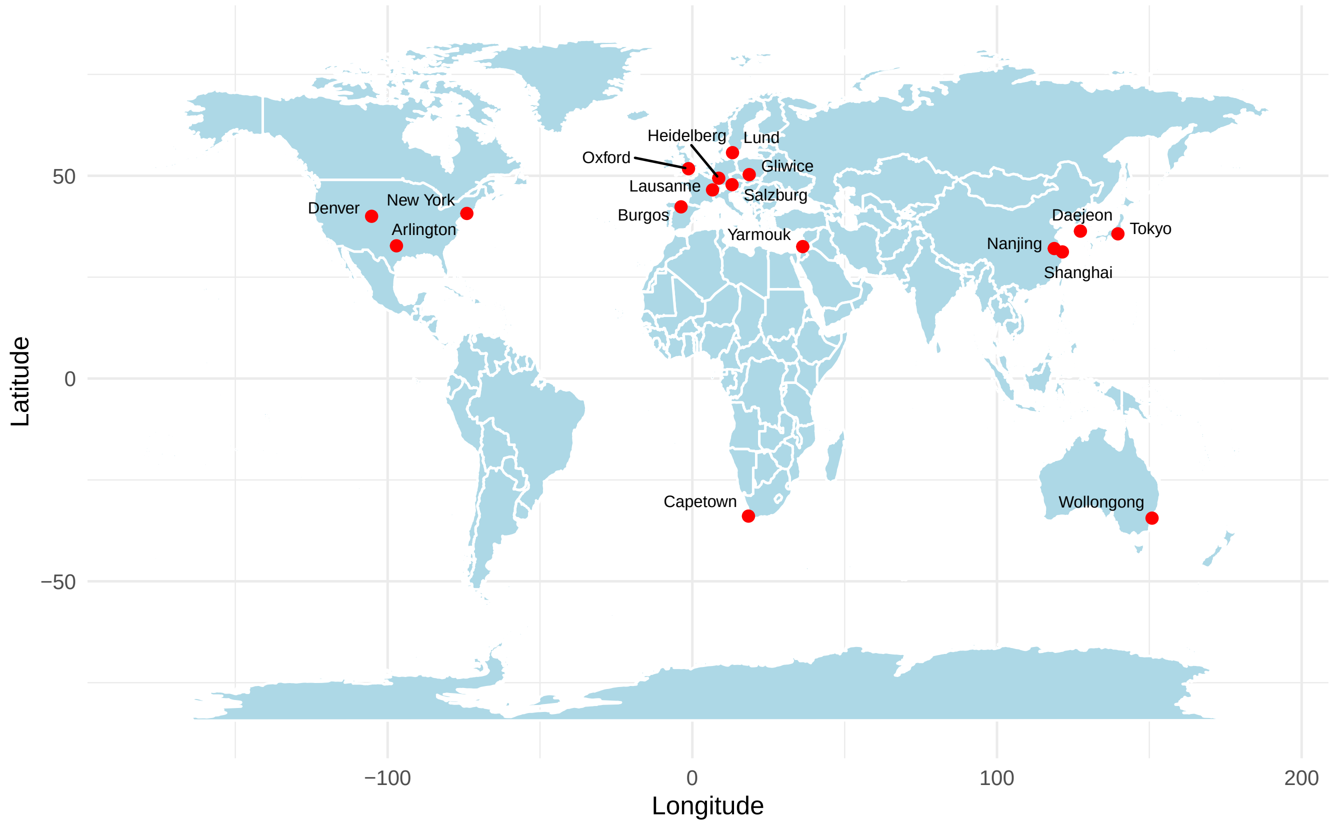

Figure 1. Affiliation of the new Editorial Board members.

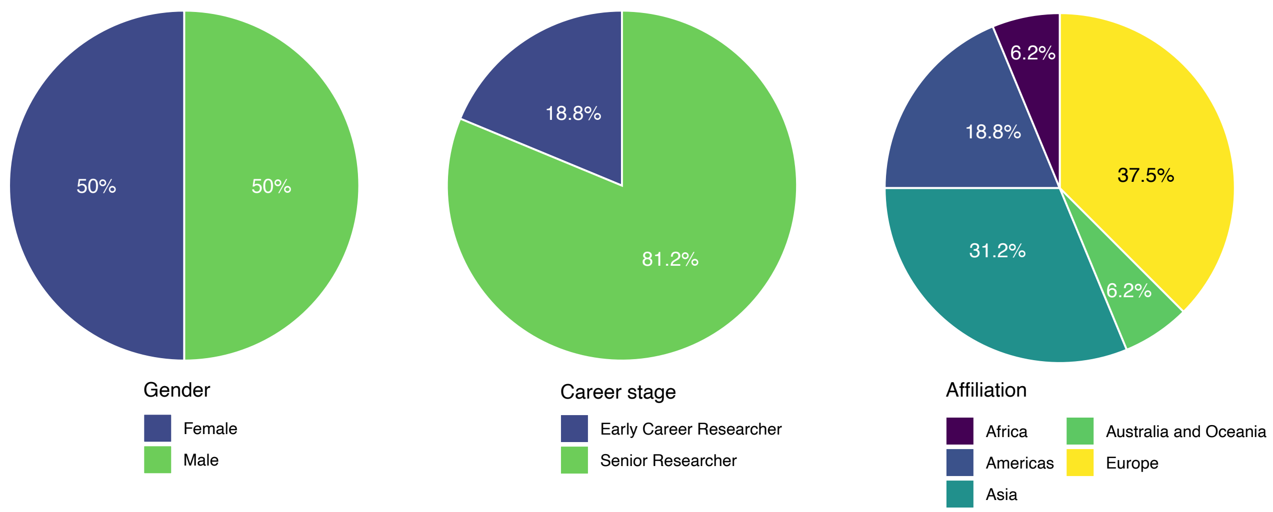

Figure 2. Gender and career stage representation as well as geographic affiliation of the new Editorial Board members. Early Career Scientists are defined as those who received their highest academic degree within the last seven years.

research published in Ancient TL. We encourage you to explore the new website and submit your latest research to Ancient TL.

The Editorial Team of Ancient TL

Ancient TL

A new reference block for field gamma spectrometry applications in ESR and luminescence dating

Mathieu Duval[1,2,3*], Miren del Val[1], María Jesús Alonso Escarza[1], Lee J. Arnold[4], Martina Demuro[4], Verónica Guilarte[5], Raju Kumar[6], Norbert Mercier[7], Jean-Luc Schwenninger[6], Chantal Tribolo[7], Gloria I. López[1,8,9,10]

[1] Centro Nacional de Investigación Sobre Evolución Humana (CENIEH), Paseo Sierra de Atapuerca 3, 09002 Burgos, Spain
[2] Australian Research Centre for Human Evolution (ARCHE), Griffith University, Nathan QLD 4111, Australia
[3] Palaeoscience Labs, Dept. Archaeology and History, La Trobe University, Melbourne Campus, Bundoora, Victoria, Australia
[4] School of Physics, Chemistry and Earth Sciences, Environment Institute, and Institute for Photonics and Advanced Sensing (IPAS), University of Adelaide, North Terrace Campus, Adelaide, SA, 5005, Australia
[5] Departamento de Didáctica de las Ciencias Experimentales. Facultad de Ciencias de la Educación y del Deporte de Melilla, Universidad de Granada. Santander 1, 52005, Melilla, Spain
[6] Research Laboratory for Archaeology and the History of Art, School of Archaeology, University of Oxford, Oxford OX1 3TG, UK
[7] Archéosciences Bordeaux, CNRS-University of Bordeaux Montaigne, Maison de l'Archéologie, Esplanade des Antilles, 33607, Pessac, France
[8] Colombian Geological Society, Carrera 32A # 25B-83, Torre 5, Local 105, Bogotá D.C., 111321, Colombia
[9] Nuclear Affairs Directorate, Colombian Geological Survey, Sede CAN, Carrera 50 # 26-20, Bogotá D.C., 111321, Colombia
[10] Leon Recanati Institute for Maritime Studies (RIMS), University of Haifa, 99 Aba Khoushy Ave, Mt Carmel, Haifa, 3498838, Israel

*Corresponding Author: mathieu.duval@cenieh.es

Received: October 15, 2024; in final form: December 13, 2024

Abstract

A new granite-doped concrete block with 60 cm × 60 cm × 60 cm dimensions has been built at CENIEH, Burgos, Spain, for dosimetry calibration and cross-referencing purposes. Independent evaluations of the block's gamma dose rate using passive Al_2O_3:C dosimeters and various field gamma spectrometer (NaI) probes produce consistent results of 1 495 ± 51 µGy a^{-1} and 1 514 ± 43 µGy a^{-1} (or 1 537 ± 19 µGy a^{-1}, depending on the evaluation procedure employed), respectively. Bulk radioelement concentrations calculated from field gamma spectrometry using the Windows method are as follows: K = 1.58 ± 0.08 %, U = 4.26 ± 0.28 ppm, and Th = 12.62 ± 0.72 ppm. This new block complements existing dosimetry reference materials accessible at other laboratories and is available for the broader trapped charge dating community to use for instrument calibration, reproducibility assessments and intercomparison studies.

Keywords: Granite-doped concrete block, Calibration, In-situ dosimetry, Field gamma spectrometry, Scintillation detectors, NaI probe, ESR dating, Luminescence dating

1. Introduction

The in situ evaluation of natural radioactivity is a crucial component of trapped charge dating methods such as Electron Spin Resonance (ESR) and Luminescence (including Optically Stimulated Luminescence [OSL], Infrared and Post-Infrared Infrared Stimulated Luminescence [IRSL, pIR-IRSL], Infrared Radiofluorescence [IR-RF] and Thermoluminescence [TL]). This is particularly important in heterogeneous sedimentary environments where it can be difficult to reliably evaluate spatially averaged gamma dose rates from laboratory analyses of discrete sediment samples alone. Passive dosimeters (e.g., OSL or TL dosimeters) or portable gamma-ray spectrometers (mostly NaI or LaBr probes) are usually employed for this purpose. The calibration of the latter is typically performed using reference blocks (e.g., Rhodes & Schwenninger, 2007; Martin, 2015), pads (e.g., Grasty & Minty, 1990), or rocks (e.g., Miallier et al., 2009) of known radioelement concentrations or gamma dose rates. While the Oxford blocks are arguably the most widely used, or at least historically significant, within the community (Bowman, 1976; Murray et al., 1978; Murray, 1981; Stokes, 1994; Rhodes & Schwenninger, 2007; Mercier & Falguères, 2007; Arnold et al., 2012; Duval & Arnold, 2013), other suitable reference blocks exist at various luminescence dating laboratories, including the Scottish Universities Environmental Research Centre (SUERC, UK) Martin (2015), the University of Bordeaux (France) (Richter et al., 2010), the University of Clermont Auvergne (France) (Miallier et al., 2009), and the Geological Survey of Israel (Porat & Halicz, 1996), amongst others. To complement these existing reference materials, the construction of a new granite-doped concrete block was initiated by one of our team members (G. I. L.) in October 2019 at the National Research Centre on Human Evolution (CENIEH) in Burgos, Spain, for dosimetric calibration purposes. Here, we provide some basic information about this new reference block, including the results of various characterisation measurements made using different methods and intercomparison studies undertaken by different research groups.

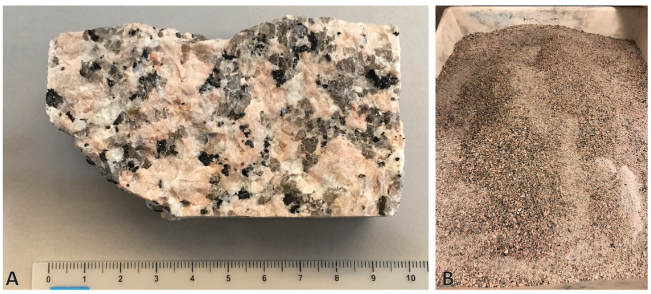

Figure 1: Picture of the Porriño granite, before (A) and after (B) crushing.

2. 2. The CENIEH reference block

In 2018, the pavement of Burgos city's main square (the Plaza Mayor) was changed to granite slabs extracted from the quarries of Porriño, Pontevedra, Spain. Commercially known as 'Rosa Porriño' (Fig. 1), this coarse-grained, phaneritic and polychromatic biotite granite, especially popular for its pinkish tone, has been widely used both nationally and internationally as an ornamental stone. It is mostly composed of quartz, potassium feldspars, plagioclase and biotite, while accessory minerals include chlorite, epidote and sericite (see detailed description in Grossi et al., 2007). The age of the granite has been constrained by U-Pb dating of selected zircons, providing an age range of 290–295 Ma, i.e., consistent with previous estimates (see Gonzalez Menéndez et al., 2017, and references therein).

In June and October 2018, the Municipality of Burgos (through the company Construcciones Ortega S.A.) donated G. I. L. a total of ten slabs of Pink Porriño granite weighing about 350 kg, which were initially sliced and then crushed to sand/gravel size (Figs. 1, A1 and A2). The construction of the block was performed on-site on 22 October 2019 using a 65 cm $\times$ 65 cm $\times$ 65 cm wooden formwork, internally coated with 5 cm-thick styrofoam slabs, and positioned onto a wooden pallet to avoid contact with the ground (Fig. A3). Cement ($\sim$125 kg), clean (washed) sand aggregate ($\sim$100 kg), crushed Porriño granite ($\sim$350 kg) and water were mixed using a clean concrete mixer. Given the limited size of the latter, two mixtures (A and B, see Fig. A4) using the same proportion of each component were prepared and the formwork was filled in four successive phases. The mixture was carefully poured into the formwork by hand, using a shovel, avoiding splashes, smearing the mixture with a trowel, avoiding bubbles and cavities. No vibration was applied. In order to evaluate the gamma dose rate and its variability across the doped block, five sub-samples of the cement-doped mixture were taken at four different stages (heights) of infilling (as described in Fig. A4), for a total of 20 dose rate control samples covering the entire cube (from edges to centre).

The final dimensions of the cubic block are 60 cm $\times$ 60 cm $\times$ 60 cm, with a horizontal 28 cm-deep cavity in its centre, constructed by inserting a 8.5 cm-diameter PVC tube (gauge: 1 mm thick) during the infilling of the cement-doped mixture. This tube serves as a cavity to accommodate cylindrical gamma spectrometer probes containing up to 3" $\times$ 3" diameter crystals (Fig. 2). The cylindrical hole does not extend all the way through the block, i.e., unlike the Oxford blocks. Additional details and pictures about the construction may be found in the Appendix.

3. Dose rate evaluation

A combination of various independent techniques has been employed to evaluate the gamma dose rate of the block, as detailed in the following sections.

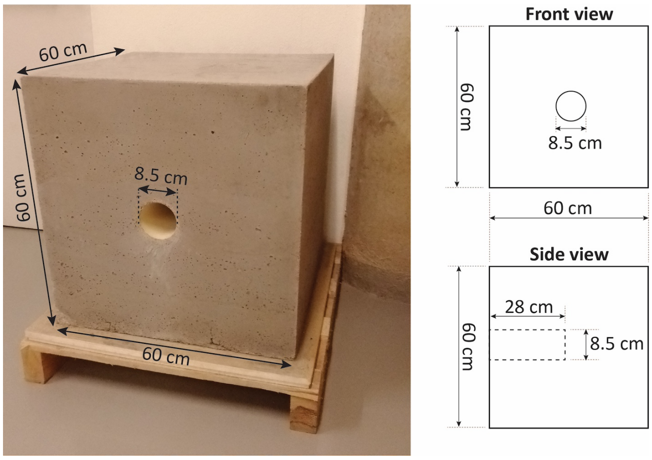

Figure 2: Picture and schematic view of the granite-doped concrete block at CENIEH, Spain.

3.1. ICP-MS/OES analysis of block sub-samples

A total of 20 samples of 15–20 g each, was collected in four successive stages during the infilling of the doped-block as described above. Consequently, each set of five samples corresponds to a given height in the cube: 12 cm (samples 1–5), 22 cm (6–10), 32 cm (11–15) and 50 cm (16–20). The wet samples were air-dried in the same conditions (i.e., in the CENIEH's second basement) and for as long as the block (1 month). Then, each dry sample was finely powdered to <1 µm using a Retsch Planetary Ball Mill PM-100 to ensure homogenisation. Radioelement concentrations were obtained by Inductively Coupled Plasma (ICP) Mass Spectrometry (U and Th) and ICP Optical (Atomic) Emission Spectrometry (K), following a 4-acid digestion procedure including hydrofluoric, nitric, perchloric and hydrochloric acids in teflon tubes. Analyses were performed by Genalysis Laboratory Services at Maddington (Perth, Australia). Individual samples were also collected from the main constituents of the block (i.e., Porriño granite, cement and sand) for comparison.

3.2. Al_2O_3:C dosimeters

One OSL dosimeter composed of two Al_2O_3:C thin chips positioned at the end of a 30 cm-long aluminium tube was left in the central hole of the block (touching the lower side of the hole) for 289 days (~9.6 months). The reading of the chips was performed at the University of Bordeaux, France, following a procedure similar to Kreutzer et al. (2018). An effective gamma dose rate was obtained after (i) removing a minor cosmic dose rate contribution, which was estimated to 21 ± 2 µGy a^{-1} (using Prescott & Hutton, 1994) given the location of the block in the basement of the building, two floors below ground level, and (ii) considering the gamma-ray attenuation induced by the aluminium tube that housed the OSL dosimeters (correction factor of 1.07 ± 0.01).

3.3. Portable gamma spectrometry probes

A series of 4π-measurements (n = 46) have been carried out in the block between 2019 and 2024 using different gamma spectrometer probes belonging to various institutions /research laboratories:

- Probe #1: 2" × 2" NaI(Tl) gamma spectrometer probe connected to a Canberra Inspector-1000 multichannel analyser (CENIEH, Spain).
- Probes #2 and #3: 2" × 2" NaI(Tl) gamma spectrometer probes connected to a Mirion-Canberra Osprey-PKG multichannel analyser (CENIEH, Spain).
- Probe #4: 2" × 2" NaI(Tl) gamma spectrometer probe connected to a Canberra Inspector-1000 multichannel analyser (Griffith University, Australia).
- Probes #5 and #6: two separate 2" × 2" NaI(Tl) gamma spectrometer probes connected to Canberra Inspector-1000 multichannel analysers (University of Adelaide, Australia).

All of these probes had been previously calibrated with the Oxford blocks (Rhodes & Schwenninger, 2007) and were used to calculate the CENIEH block gamma dose rate using either the Threshold method (probes #1–4) or Windows method (probes #5–6), following the procedures described in Duval & Arnold (2013) and Arnold et al. (2012), respectively. Additionally, the Matlab-based OxGamma program (Kumar et al., 2022) was employed in parallel for selected spectra (probes #1 to #4) to determine the block gamma dose rate via the Threshold approach, in order to evaluate any potential bias related to the specific evaluation procedure used.

4. Results and discussion

4.1. ICP-MS/OES analysis of block samples

ICP-MS/OES analytical results show significant variability in radioelement concentrations (relative standard deviations between 27 % and 44 %), with U, Th and K ranging from 3.42–7.39 ppm, 7.15–28.1 ppm and 1.11–3.59 %, respectively (Table 1). The U and K values are within the range of radioelement concentrations measured from the main individual components of the block, i.e., the pure granite, sand aggregate and cement samples. In contrast, many samples from the block show a significantly higher Th concentration (17 ppm on average) than in the reference samples, which have values of 10.5 ppm (granite) to 15 ppm (cement) (Table 1). This unexpected outcome might result from the heterogeneity of the rock, suggesting that Th-bearing minerals may be noticeably underrepresented in the single sample of the Porriño granite analysed by ICP. This may also explain why the individual sample from the cement returned higher Th concentration than the granite.
Using the dose rate conversion factors from Guérin et al. (2011) and assuming infinite matrix conditions and a water content of 0 %, a mean gamma dose rate of

Table 1: Radioelement concentrations measured by ICP-MS/OES. Uncertainties are shown at 1σ. Samples 1–10 and 11–20 were collected from mixtures A and B, respectively. Samples 1–5, 6–10, 11–15 and 16–20 correspond to different phases of infill (see further details in Appendix A4).

Sample	**Height [cm]**[1]	**U [ppm]**	**Th [ppm]**	**K [%]**
LM-19276-01-1	12	6.22 ± 0.16	25.31 ± 1.02	3.42 ± 0.10
LM-19276-01-2	12	6.41 ± 0.16	27.20 ± 1.09	3.52 ± 0.11
LM-19276-01-3	12	7.39 ± 0.19	27.63 ± 1.11	3.46 ± 0.10
LM-19276-01-4	12	5.73 ± 0.15	23.59 ± 0.95	3.49 ± 0.10
LM-19276-01-5	12	5.59 ± 0.14	22.53 ± 0.91	3.59 ± 0.11
LM-19276-01-6	22	6.94 ± 0.18	28.10 ± 1.13	3.17 ± 0.09
LM-19276-01-7	22	5.77 ± 0.15	21.76 ± 0.88	3.30 ± 0.10
LM-19276-01-8	22	5.65 ± 0.14	20.54 ± 0.83	3.05 ± 0.09
LM-19276-01-9	22	6.14 ± 0.16	22.70 ± 0.91	3.29 ± 0.10
LM-19276-01-10	22	6.34 ± 0.16	22.15 ± 0.89	3.09 ± 0.09
LM-19276-01-11	32	4.22 ± 0.11	11.65 ± 0.47	1.75 ± 0.05
LM-19276-01-12	32	3.81 ± 0.10	12.77 ± 0.51	1.57 ± 0.05
LM-19276-01-13	32	3.90 ± 0.10	13.69 ± 0.55	1.67 ± 0.05
LM-19276-01-14	32	3.84 ± 0.10	10.32 ± 0.42	1.73 ± 0.05
LM-19276-01-15	32	4.28 ± 0.11	16.21 ± 0.65	1.64 ± 0.05
LM-19276-01-16	50	3.95 ± 0.10	9.40 ± 0.38	1.19 ± 0.04
LM-19276-01-17	50	3.42 ± 0.09	7.15 ± 0.29	1.12 ± 0.03
LM-19276-01-17[2]	50	3.46 ± 0.09	7.33 ± 0.30	1.12 ± 0.03
LM-19276-01-18	50	3.85 ± 0.10	10.61 ± 0.43	1.16 ± 0.03
LM-19276-01-19	50	3.53 ± 0.09	7.68 ± 0.31	1.11 ± 0.03
LM-19276-01-20	50	3.44 ± 0.09	9.02 ± 0.36	1.23 ± 0.04
Mean ± 1 std. dev. (%)	12–50	4.95 ± 1.32 (26.7 %)	17.02 ± 7.48 (44.0 %)	2.32 ± 1.02 (44.1 %)
Min	12–50	3.42 ± 0.09	7.15 ± 0.29	1.11 ± 0.03
Max	12–50	7.39 ± 0.19	28.10 ± 1.13	3.59 ± 0.11
Mean ± 1 std. dev. (%)	12	3.49 ± 0.07 (1.9 %)	25.25 ± 2.21 (8.8 %)	6.27 ± 0.71 (11.4 %)
Mean ± 1 std. dev. (%)	22	3.18 ± 0.11 (3.6 %)	23.05 ± 2.93 (12.7 %)	6.17 ± 0.51 (8.3 %)
Mean ± 1 std. dev. (%)	32	1.67 ± 0.07 (4.2 %)	12.93 ± 2.23 (17.2 %)	4.01 ± 0.22 (5.5 %)
Mean ± 1 std. dev. (%)	50	1.15 ± 0.05 (4.4 %)	8.36 ± 1.46 (17.4 %)	3.54 ± 0.18 (5.0 %)
Main constituents				
Porriño granite		11.63 ± 0.30	10.52 ± 0.30	2.83 ± 0.08
Sandy aggregate		2.46 ± 0.06	2.15 ± 0.06	0.30 ± 0.01
Cement		1.72 ± 0.04	15.09 ± 0.04	2.72 ± 0.08

[1] Height corresponds to the approximated vertical distance (in cm) from the bottom of the cube.
[2] Note that two sub-samples of sample 17 were collected. The two subsamples return similar radioelement concentrations (within error).

1 926 ± 463 μGy a^{-1} may be tentatively calculated for the whole block from the mean radioelement concentrations (Table 1). This value should however be treated with extreme caution, as it is unlikely to provide a reliable estimate of the true gamma dose rate given the significant variability observed between the 20 sub-samples from the block (Table 1). We presently suspect that this variability may mostly be due to the relative inhomogeneity in the mixing of the various components of the block (see also Bowman, 1976; Murray, 1981, for further information on that specific matter), resulting in the spatial heterogeneity of radioelement distribution. Interestingly, this hypothesis is supported by the ICP results from each set of samples collected at increasing height in the block: they show a significant vertical gradient in radioelement concentrations, with lower values towards the top of the block (U: 3.5 ppm to 1.2 ppm; Th: 25.3 ppm to 8.4 ppm; K: 6.3 % to 3.5 %; Table 1). Moreover, within a given set of samples (i.e., corresponding to a given height), radioelement concentrations also show a non-negligible variability (1 relative standard deviation) of 1.9–4.4 %, 8.8–17.4 % and 5.0–11.4 % for U, Th and K, respectively (Table 1). Consequently, the block shows an overall (vertical and horizontal) inhomogeneity. Despite our best efforts to ensure a relative homogeneous mixing, empirical data indicate that this was not achieved (see also how the two mixtures A and B compare in terms of radioelement concentrations, i.e., samples 1–10 vs. 11–20 in Table 1). We do acknowledge that our precautions were probably not as thorough as those em-

ployed for the construction of the Oxford Blocks (Bowman, 1976; Murray et al., 1978; Murray, 1981), and we would welcome any feedback, perhaps resulting from similar experiences, from the LED community on this matter.

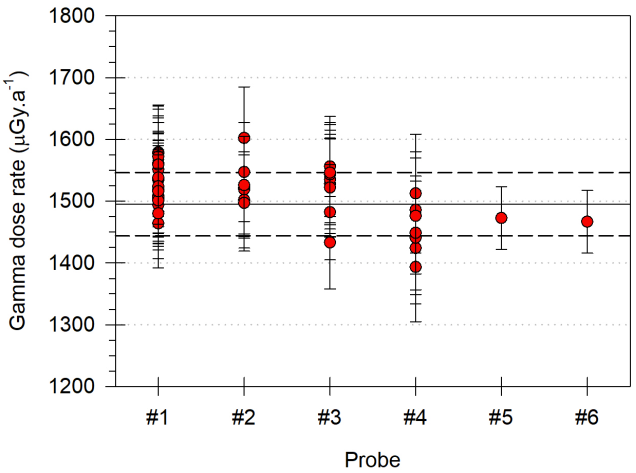

Figure 3: Graphical overview of the gamma dose rate measured for the granite-doped block with NaI(Tl) probes #1 to #6. Numerical values may be found in Table 2. The horizontal solid and short dash lines represent the value and associated 1σ uncertainties obtained from the Al_2O_3:C dosimeters (1 495 ± 51 µGy a^{-1}).

Table 2 (next page): Overview of the granite block gamma dose rate values measured over a five-year period with various NaI(Tl) gamma spectrometer probes. Gamma dose rate values have been calculated with the Threshold method following two different procedures: (i) Arnold et al. (2012) and Duval & Arnold (2013), and (ii) OxGamma (Kumar et al., 2022). The gamma dose rate ratios (FGS/dosimeter) were obtained by comparing the field gamma spectrometer (FGS) dose rates with the independent values obtained using the Al_2O_3:C dosimeters (1 495 ± 51 µGy a^{-1}). Note that a minor internal gamma dose rate contribution from the NaI(Tl) probe itself (∼10 µGy a^{-1}, corresponding to <0.1 % of the measured gamma dose rate) was subtracted from all values derived using the procedure of Duval & Arnold (2013), unlike for the OxGamma results. Uncertainties are shown at 1σ. Key: n.c. = not calculated.

4.2. Al_2O_3:C dosimeters

A mean effective gamma dose rate of 1 495 ± 51 µGy a^{-1} was obtained from the two Al_2O_3:C chips. The relative associated error (3.4 %) includes the calibration source error (2.9 %), and its magnitude illustrates the limited dose variability among the chips, which returned consistent values differing by <2 %.

4.3. Portable gamma spectrometry

All measurements made using the six different gamma spectrometer probes return consistent values (within ± 2.8 % on average), regardless of the probe employed (Tables 2–3; Fig. 3). A mean Threshold-based gamma dose rate of 1 514 ± 43 µGy a^{-1} (1 s.d.) can be calculated from all measurements (n = 44) made with probes #1 to #4. Each probe shows relatively high measurement repeatability, with a relative standard deviation of <4 % in the gamma dose rate values (probe #1 = 2.0 % [$n = 20$]; probe #2 = 2.3 % [$n = 7$]; probe #3 = 2.5 % [$n = 9$]; probe #4: 2.7 % [$n = 8$]). These values likely reflect the inherent precision of the gamma spectrometers used in this study, and are consistent with the reproducibility uncertainty (2.1 %) previously estimated by Arnold et al. (2012) for a similar gamma spectrometer. The mean Threshold-based gamma dose rate values obtained for each probe are in close agreement at 1σ: 1 527 ± 31 µGy a^{-1} (#1), 1 531 ± 35 µGy a^{-1} (#2), 1 519 ± 38 µGy a^{-1} (#3), 1 459 ± 39 µGy a^{-1} (#4). The slightly lower mean value obtained for probe #4 is especially impacted by a single low outlying measurement (2308GU, Table 2), given the small size of the data set (n = 8). An average gamma dose rate of 1 468 ± 31 µGy a^{-1} may be calculated instead for this probe when excluding this measurement (Table 2), which is in closer agreement with the results obtained from the other probes.

The Threshold-based gamma dose rates obtained using OxGamma are consistent with (i.e., within error of) those calculated using the procedures described in Duval & Arnold (2013) for all probe measurements. The corresponding results differ by 1–4 % on average for a given probe (Table 2), by about 1.5 % when considering all measurements (n = 44), and the individual deviation observed for each spectrum is consistently <5 % (with three exceptions). The differences observed partly originate from the subtraction of the gamma dose rate contribution from the NaI(Tl) probe itself (∼10 µGy a^{-1}, corresponding to <0.1 % of the measured gamma dose rate), which is not considered by OxGamma, unlike Duval & Arnold (2013). When including this component in both evaluation procedures, the relative difference drops from 1.5 % to <1 % on average when considering all measurements (Table 2). Finally, it can be observed from Table 2 that OxGamma offers an overall higher measurement repeatability, with gamma dose rate values showing slightly lower variability, and hence higher consistency, for a given probe (probe #1 = 1.3 vs. 2.0 % [$n = 20$]; probe #2 = 0.8 vs. 2.3 % [$n = 7$]; probe #3 =

Date	Probe	Spectrum ID	Duval and Arnold (2013) Gamma dose rate [µGy a^{-1}]	Duval and Arnold (2013) Gamma dose rate ratio (FGS/dosimeter)	OxGamma Gamma dose rate [µGy a^{-1}]	OxGamma Gamma dose rate ratio (FGS/dosimeter)
Nov-19	#1	1965N	1 505 ± 74	1.01	1 567 ± 78	1.05
Dec-19	#1	1972N	1 519 ± 75	1.02	1 563 ± 78	1.05
Feb-20	#1	2010N	1 579 ± 77	1.06	1 566 ± 78	1.05
Mar-20	#1	2012N	1 561 ± 77	1.04	1 566 ± 78	1.05
May-20	#1	2013N	1 494 ± 73	1.00	1 557 ± 78	1.04
Jun-20	#1	2017N	1 534 ± 75	1.03	1 559 ± 78	1.04
Jul-20	#1	2019N	1 551 ± 76	1.04	1 577 ± 79	1.05
Aug-20	#1	2021N	1 577 ± 77	1.05	1 562 ± 78	1.04
Sep-20	#1	2023N	1 572 ± 77	1.05	1 577 ± 79	1.06
Oct-20	#1	2025N	1 536 ± 75	1.03	1 542 ± 77	1.03
Nov-20	#1	2027N	1 509 ± 74	1.01	1 534 ± 77	1.03
Dec-20	#1	2028N	1 464 ± 72	0.98	1 526 ± 76	1.02
Jan-21	#1	2102N	1 523 ± 75	1.02	1 528 ± 76	1.02
Feb-21	#1	2104N	1 559 ± 76	1.04	1 524 ± 76	1.02
Mar-21	#1	2105N	1 538 ± 75	1.03	1 524 ± 76	1.02
Apr-21	#1	2111N	1 506 ± 74	1.01	1 544 ± 77	1.03
May-21	#1	2118N	1 524 ± 75	1.02	1 529 ± 76	1.02
Aug-21	#1	2123N	1 501 ± 74	1.00	1 526 ± 76	1.02
Oct-21	#1	2132N	1 516 ± 74	1.01	1 522 ± 76	1.02
Nov-21	#1	2169N	1 480 ± 73	0.98	1 546 ± 77	1.03
Oct-22	#2	2212A	1 522 ± 79	1.02	1 519 ± 76	1.02
Jun-23	#2	2322A	1 519 ± 79	1.02	1 518 ± 76	1.02
Aug-23	#2	2326A	1 502 ± 78	1.00	1 517 ± 76	1.01
Aug-23	#2	2325A	1 497 ± 78	1.00	1 531 ± 77	1.02
Feb-24	#2	2413A	1 547 ± 80	1.03	1 545 ± 77	1.03
Jun-24	#2	2439A	1 602 ± 83	1.07	1 510 ± 76	1.01
Aug-24	#2	2449A	1 526 ± 79	1.02	1 524 ± 76	1.02
Sep-22	#3	2211B	1 556 ± 81	1.04	1 531 ± 77	1.02
Oct-22	#3	2212B	1 528 ± 80	1.02	1 525 ± 76	1.02
Jun-23	#3	2311B	1 535 ± 80	1.03	1 562 ± 78	1.04
Aug-23	#3	2314B	1 543 ± 81	1.03	1 540 ± 77	1.03
Aug-23	#3	2313B	1 482 ± 77	0.99	1 541 ± 77	1.03
Aug-23	#3	2315B	1 522 ± 79	1.02	1 539 ± 77	1.03
Feb-24	#3	2401B	1 522 ± 80	1.02	1 541 ± 77	1.03
Jun-24	#3	2408B	1 546 ± 81	1.03	1 521 ± 76	1.02
Aug-24	#3	2417B	1 433 ± 75	0.96	1 536 ± 77	1.03
Sep-21	#4	2115GU	1 486 ± 94	0.99	1 520 ± 76	1.01
Oct-21	#4	2120GU	1 424 ± 90	0.95	1 510 ± 76	1.00
Jul-22	#4	2224GU	1 441 ± 92	0.96	1 520 ± 76	1.01
Jul-22	#4	2225GU	1 449 ± 92	0.97	1 514 ± 76	1.00
Aug-23	#4	2308GU	1 393 ± 89	0.93	1 518 ± 76	1.00
Jul-24	#4	2401GU	1 512 ± 96	1.01	1 518 ± 77	1.00
Jul-24	#4	2402GU	1 476 ± 94	0.99	1 521 ± 76	1.01
Sep-24	#4	2409GU	1 488 ± 95	1.00	1 511 ± 76	1.00
Mean ± 1 std. dev. (%)						
	#1		1 527 ± 31 (2.0 %)	1.02	1 547 ± 20 (1.3 %)	1.03
	#2		1 531 ± 35 (2.3 %)	1.02	1 523 ± 11 (0.8 %)	1.02
	#3		1 519 ± 38 (2.5 %)	1.02	1 537 ± 12 (0.8 %)	1.03
	#4		1 459 ± 39 (2.7 %)	0.98	1 517 ± 4 (0.3 %)	1.01
	All		1 514 ± 43 (2.9 %) [1 524 ± 43][1]	1.02	1 537 ± 19 (1.2 %)	1.03

[1] Average value including the minor internal component from the probe (10 µGy a^{-1}), to facilitate a direct comparison with the corresponding OxGamma result.

Table 3: Radioelement concentrations measured by field gamma spectrometry using the Windows method outlined in Arnold et al. (2012). Gamma dose rates have been calculated using the dose rate conversion factors of Guérin et al. (2011) and a water content of 0 %. No internal gamma dose rate contribution from the NaI(Tl) probe itself was considered here. The gamma dose rate ratios (FGS/dosimeter) were obtained by comparing the field gamma spectrometer (FGS) dose rates with the independent values obtained using the Al_2O_3:C dosimeters (1 495 ± 51 µGy a^{-1}). Elemental concentration uncertainties and gamma dose rate uncertainties are shown at 1σ.

Date	Probe	Spectrum	U [ppm]	Th [ppm]	K [%]	Gamma dose rate [µGy a^{-1}]	Gamma dose rate ratio (FGS/dosimeter)
Jul-22	#5	2275a	4.30 ± 0.28	12.71 ± 0.73	1.56 ± 0.08	1 473 ± 51	0.99
Jul-24	#6	2420c	4.23 ± 0.28	12.53 ± 0.72	1.61 ± 0.09	1 467 ± 51	0.98

0.8 vs. 2.5 % [$n = 9$]; probe #4: = 0.3 vs. 2.7 % [$n = 8$]). In summary, these results provide confidence that the two independent evaluation procedures are directly comparable and the resultant gamma dose rates are reproducible.

The gamma dose rate values calculated using the Windows method (Arnold et al., 2012) for probes #5 and #6 (1 473 ± 51 µGy a^{-1} and 1 467 ± 51 µGy a^{-1}, respectively; Table 3) are not only consistent with each other (differing by <1 %), but are also in agreement at 1σ with the various Threshold-based gamma dose rate values obtained for probes #1 to #4 obtained with either Duval & Arnold (2013)'s procedure or OxGamma (Table 2). Moreover, the following average radioelement concentrations and associated errors may be calculated from these two independent measurements: K = 1.58 ± 0.08 %, U = 4.26 ± 0.28 ppm, Th = 12.62 ± 0.72 ppm. Unlike the average radioelement concentrations derived from ICP analyses of block sub-samples (section 4.1), these results may be regarded as reliable spatially averaged estimates of the bulk radioelement concentrations when performing dosimetry evaluations in the central hole of the block. To sum up, independent dosimetry assessments made using different gamma probes and data evaluation procedures (Threshold vs. Windows; Duval & Arnold (2013) vs. OxGamma) return consistent results and support the robustness of the combined data set.

4.4. Comparison of dosimetry approaches

A comparison of the various gamma dose rate values obtained independently or semi-independently using different dosimetry evaluations provides useful insights into their accuracy. In this context, the mean Threshold-based gamma dose rate of 1 514 ± 43 µGy a^{-1} (1 s.d.) calculated from all measurements (Duval & Arnold (2013)'s evaluation procedure) made with probes #1 to #4 is in excellent agreement with the independent gamma dose rate (1 495 ± 51 µGy a^{-1}) obtained from the Al_2O_3:C dosimeter (deviation ∼2 %). Additionally, the deviation observed for each spectrum does not exceed 5 % of the Al_2O_3:C dosimeter gamma dose rate in most cases (with a few exceptions (n = 3); Table 2), and it is consistently <10 % for all spectra, demonstrating sufficient reproducibility for both techniques (Fig. 3).
The two Windows-based gamma dose rate values of 1 473 ± 51 µGy a^{-1} (probe #5) and 1 467 ± 51 µGy a^{-1} (probe #6) are also consistent at 1σ with the Al_2O_3:C gamma dose rate estimate (1 495 ± 51 µGy a^{-1}, with the two datasets differing by only ∼2 %. To sum up, all in situ gamma dose rate results obtained using NaI probe gamma spectrometry and Al_2O_3:C dosimeters are within close range of each other. Finally, it is noteworthy that both the NaI gamma probes and the Al_2O_3:C dosimeters produce gamma dose rates that are significantly lower (by >400 µGy a^{-1}) than that initially estimated from all the ICP analyses; though the two sets of results actually overlap at 1σ given the large uncertainty associated with the ICP measurements. This confirms that the latter should not be regarded as a reliable estimate of the true gamma dose rate of the block at the central hole measurement position, mostly owing to spatial heterogeneity in the granite-doped concrete block mixture, although we cannot discard that other sources of uncertainty may also be possibly involved (see discussion in Bowman, 1976; Murray, 1981).

5. Conclusion

We present a new dosimetry reference block that complements a range of similar structures available at various luminescence and ESR dating laboratories around the world. Despite apparent non-negligible heterogeneity in the spatial distribution of radioelements in the block as suggested by the significant variability of the ICP analytical results from 20 strategically-collected samples, the gamma dose rates measured in the central hole position with two independent techniques (Al_2O_3:C dosimeters and NaI probe gamma spectrometry) and using various evaluation procedures are all within close range of each other. The consistency of these results suggests that the true gamma dose rate at the centre of the block has been properly constrained, although efforts are ongoing to further refine this initial evaluation through a combination of experimental and modeling procedures. Based on the experience acquired through decades of investigations around the Oxford Blocks (e.g., Bowman, 1976; Murray et al., 1978; Murray, 1981; Rhodes & Schwenninger, 2007, and references therein), we also acknowledge that several aspects of the CENIEH block will deserve further attention (e.g., density, disequilibrium, water content, spatial heterogeneity) in order to ensure its exhaustive characterization. In this regard, we welcome future collaborative initiatives or any scientific inputs on this matter. The CENIEH reference block is made available to all members of the trapped charge dating community for instrument calibration and reproducibility assessments, including intercomparison studies with similar dosimetry reference materials at other laboratories.

Acknowledgements

We thank Carlos Pérez Garrido, CENIEH, for his contribution to the gamma dose rate evaluation from field gamma spectra, as well as David Martinez Asturias, Carlos Sáiz Dominguez, Jaime Torres, CENIEH, and Adolfo Alonso and his team “Construcciones A10” for their invaluable help with the construction of the block. A major thank you to "Construcciones Ortega S.A.", the Burgos company commissioned by the Burgos City Council to renovate the pavement of its emblematic Plaza Mayor, for kindly donating the slabs of the pink Porriño granite to G. I. L., without which this block could not have been made. Raju Kumar acknowledges support from UK Research and Innovation (Natural Environment Research Council grant reference NE/T001313/1). This research benefitted from the scientific framework given by the University of Bordeaux's IdEx "Investments for the Future" program / GPR "Human Past". We would also like to extend our thanks to the reviewer and editor for their constructive comments on the manuscript.

References

Arnold, L. J., Duval, M., Falguères, C., Bahain, J.-J., and Demuro, M. *Portable gamma spectrometry with cerium-doped lanthanum bromide scintillators: Suitability assessments for luminescence and electron spin resonance dating applications*. Radiation Measurements, 47(1): 6–18, 2012.

Bowman, S. *Thermoluminescent Dating: The Evaluation of Radiation Dosage (Appendix A.5. Environmental Dosimetry)*. PhD thesis, University of Oxford, 1976.

Duval, M. and Arnold, L. J. *Field gamma dose-rate assessment in natural sedimentary contexts using LaBr3 (Ce) and NaI (Tl) probes: A comparison between the “threshold” and “windows” techniques*. Applied Radiation and Isotopes, 74: 36–45, 2013.

Gonzalez Menéndez, L., Gallastegui Suárez, G., Cuesta Fernández, A., Montero, P., Rubio Ordóñez, A., Molina, J., and Bea Barredo, F. *Petrology and geochronology of the Porriño late-Variscan pluton from NW Iberia. A model for post-tectonic plutons in collisional settings*. Geologica Acta, 15(4): 283–304, 2017.

Grasty, R. L. and Minty, B. R. S. *A Guide to the Techncial Specifications for Airborne Gamma-ray Surveys*. Citeseer, 1990. ISBN 0642223661.

Grossi, C. M., Alonso, F. J., Esbert, R. M., and Rojo, A. *Effect of laser cleaning on granite color*. Color Research & Application, 32(2): 152–159, 2007.

Guérin, G., Mercier, N., and Adamiec, G. *Dose-rate conversion factors: update*. Ancient TL, 29: 5–8, 2011.

Kreutzer, S., Martin, L., Guérin, G., Tribolo, C., Selva, P., and Mercier, N. *Environmental dose rate determination using a passive dosimeter: Techniques and workflow for α-Al_2O_3:C chips*. Geochronometria, 45(1): 56–67, 2018.

Kumar, R., Frouin, M., Gazack, J., and Schwenninger, J.-L. *OxGamma: A MATLAB based application for the analysis of gamma-ray spectra*. Radiation Measurements, 154: 106761, 2022.

Martin, L. *Caractérisation et modélisation d'objets archéologiques en vue de leur datation par des méthodes paléo-dosimétriques: simulation des paramètres dosimétriques sous Geant4*. PhD thesis, Université Michel de Montaigne - Bordeaux III, 2015.

Mercier, N. and Falguères, C. *Field gamma dose-rate measurement with a NaI(Tl) detector: Re-evaluation of the "threshold" technique*. Ancient TL, 25: 1–4, 2007.

Miallier, D., Guérin, G., Mercier, N., Pilleyre, T., and Sanzelle, S. *The Clermont radiometric reference rocks: A convenient tool for dosimetric purposes*. Ancient TL, 27: 37–43, 2009.

Murray, A. *Environmental radioactivity studies relevant to thermoluminescence dating*. PhD thesis, University of Oxford, 1981.

Murray, A., Bowman, S., and Aitken, M. *Evaluation of the gamma dose-rate contribution*. Journal of the European Study Group on Physical, Chemical and Mathematical Techniques Applied to Archaeology (PACT), 2: 84–96, 1978.

Porat, N. and Halicz, L. *Calibrating the luminescence dating laboratory*. Geological Survey of Israel Current Research, 10: 111–116, 1996.

Prescott, J. R. and Hutton, J. T. *Cosmic ray contributions to dose rates for luminescence and ESR dating: large depths and long-term time variations*. Radiation Measurements, 23(2–3): 497–500, 1994.

Rhodes, E. and Schwenninger, J.-L. *Dose rates and radioisotope concentrations in the concrete calibration blocks at Oxford*. Ancient TL, 25: 5–8, 2007.

Richter, D., Dombrowski, H., Neumaier, S., Guibert, P., and Zink, A. C. *Environmental gamma dosimetry with OSL of α-Al_2O_3:C for in situ sediment measurements*. Radiation Protection Dosimetry, 141(1): 27–35, 2010.

Stokes, S. *Optical dating of selected Late Quaternary aeolian sediments from the Southwestern United States*. PhD thesis, University of Oxford, 1994.

Reviewer

Ed Rhodes

Reviewer comment

The doped concrete block described in this paper represents a highly valuable addition to the calibration toolset for luminescence dating laboratories. Portable gamma spectrometry offers many benefits, with only relatively minor difficulty, but reliable calibration is important. I feel that having a secure value for the total gamma dose rate, often determined by the threshold method typically with relatively high precision, or using the window approach that provides a determination of the apparent concentrations of U, Th and K, is key to good calibration. This block delivers this with a convincing set of determinations using both Al_2O_3:C chips and a suite of six pre-calibrated NaI probes measured with four different portable gamma spectrometers, displaying a high degree of internal consistency. The apparent discrepancy between the direct gamma dose rate measurements described above and ICP determinations of U, Th and K content from 20 subsamples collected during manufacture illustrate how hard it is to achieve homogeneity with real world materials. The authors note some similarity in this discrepancy with similar observations made during the construction of the Oxford blocks during the 1970s.

Appendix

Figure A1: Pink Porriño granite slabs upon arrival at the CENIEH, as donated to G. I. L. by Burgos' Municipality (October 31, 2018).

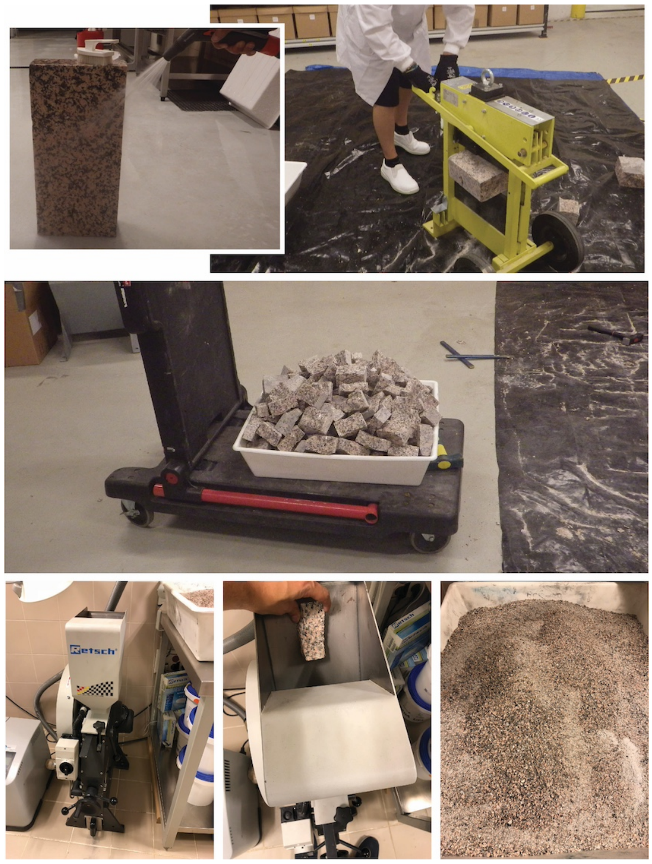

Figure A2: Slicing and crushing the Porriño granite slabs. Each slab was thoroughly cleaned of any external dirt. A guillotine-type hydraulic cutting machine was used to slice each slab into hand-sized pieces, manageable enough to crush using a laboratory jaw crusher. Care was taken to avoid cross-contamination from the ground and surroundings during slicing (a clean black tarp was spread out to contain the sliced slabs).

Figure A3: Construction of the Porriño granite-doped block (October 22, 2019). Once filled with the mixture, the plywood formwork was reinforced with strongly attached thick wooden boards to hold it together while the concrete block air-dried. It took the mixture almost 1 month to completely dry.

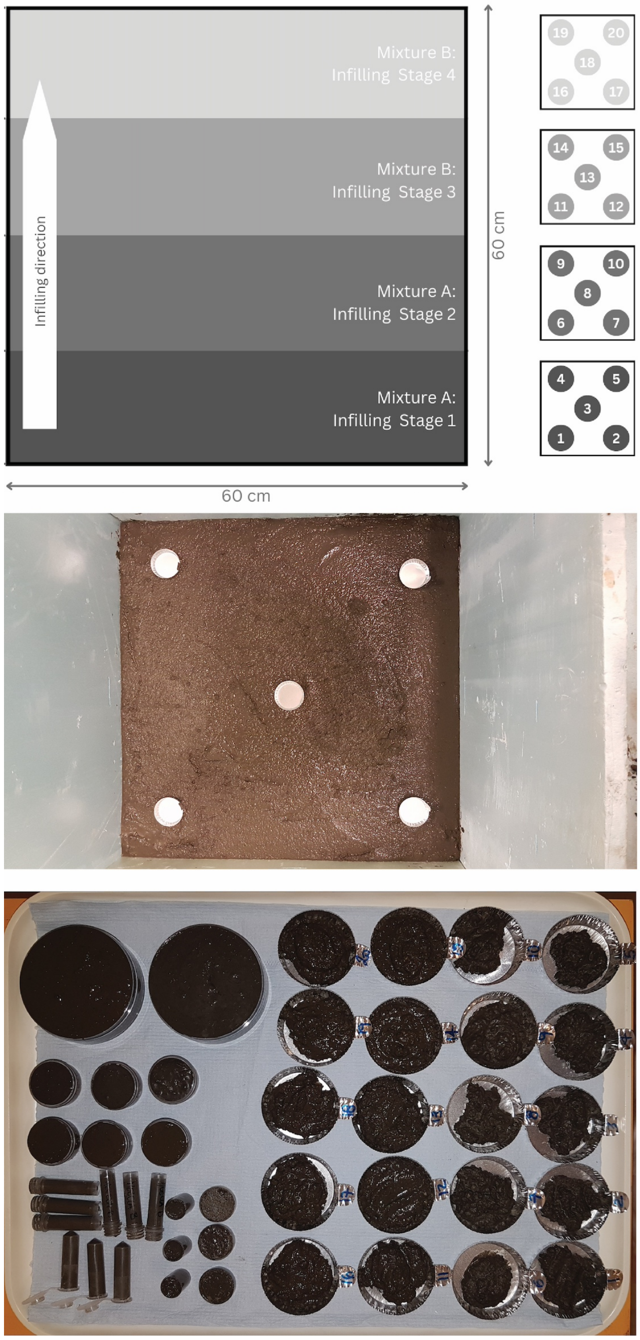

Figure A4: Sampling of the Porriño granite-doped block. Five sub-samples were taken from all four corners and centre of the formwork as it was being infilled with the mixture (two mixtures A and B poured in a total of four successive phases), for a total of 20 dose rate control samples. The sub-sampling intervals were at 12 cm from the bottom of the formwork; 22 cm of infilling (corresponding to the base of the horizontal PVC tube inserted to maintain a 8.5 cm-diameter $\times$ 28 cm-long cavity at the centre of the doped cube); 32 cm of infilling; and at 50 cm of infilling, just 10 cm below the top of the cube.

Thesis Abstracts

Index

Diana Chourio Camacho

Late Quaternary incision dynamics and valley bottom geometry within the Seine River catchment

March 2024

PSL University/MINES Paris/Centre de Géosciences, Fontainebleau, France

Degree: Ph.D.

Supervisors: Jean-Louis Grimaud, Hélène Tissoux, Paul Bessin, Mark Noble

Thanks to the use of paleodosimetric dating methods (ESR, OSL), this thesis contributes to better understand the chronology of the valley evolution and sediment transfer within the Seine River catchment and its major tributaries (Oise, Marne, Aube, Yonne, Loing and Eure rivers) during the Late Quaternary period. The valley bottom along the Seine catchment is variable in width, providing space for sediment accumulation during alluvial transfer. The alluvial deposits of the Seine River are mainly composed of quartz, which results from the alteration and erosion of the bedrock through which the river flows. This makes it possible to apply dating methods on quartz grains to estimate the phases of alluvial deposits following the incisions associated with major Quaternary climatic fluctuations. The aim of this thesis is first to propose a chronology of the valley bottom's infill and second to determine the residence timescale within the valleys based on the geometry at the bedrock alluvium interface.

For this, a total of 21 samples were collected from different sites within the Seine catchment in a fluvial environment, principally in valley bottoms, along their edges or in some fossil terraces. These samples were dated combining both the electron spin resonance (ESR) and optically stimulated luminescence (OSL) methods on optically bleached quartz grains provided by alluvial sediments. Seven samples were dated coupling both ESR and OSL methods, six using the ESR method and eight using the OSL method. Both methods are based on the same physical principle: the accumulation of electrons in trapping structures within the quartz lattice over time due to natural radiation.

Sample ages were determined as the ratio of total dose received since their deposition (equivalent dose D_e which is expressed in Gy) to the received dose calculated for one year (annual dose D_a, expressed in µGy a^{-1}). The annual dose for all samples was determined considering the content of radioactive elements such as U, Th and daughters, and K in the field using a portable NaI γ-spectrometer and in the laboratory (High Purity Ge detector). The same D_a value was used for both ESR and OSL ages calculation. In contrast, the two methods differ in D_e determination. The D_e for ESR was calculated using the multiple aliquot additive (MAA) dose method, while for OSL the D_e was determined considering the single-aliquot-regenerative-dose (SAR) approach. ESR ages were determined by the multicentre approach using the Al, TiLi and TiH centres. A validation criterion of the dose response curves was performed regarding the comparison between the experimental points and the theoretical growth curve. A particular emphasis was given on the points with lower irradiation doses, with a special focus on allowing the curve to pass through the "natural" point.

The results of the ESR-OSL dating of sediments are predominantly associated with the glacial-interglacial Quaternary cycles. Along the valley bottom the returned ages recorded at least two Marine Isotopic Stages (MIS 6 and MIS 2). It is known that at the end of the Weichselian glaciation (MIS 2) erosion was less powerful than at the end of MIS 6. Therefore, it is possible that the deposits in the valley bottom from MIS 6 were not entirely removed during the Weichselian glaciation MIS 2, preserving deposits from MIS 6 in the valley bottom. Strath terrace deposits dated in this work provide additional constraints on the ages of the Seine valley formation and on incision rates since the Middle Pleistocene. Overall, the incision rates estimated from these terraces are in good agreement with the long-term incision rates known in the Paris Basin (50–60 m Ma^{-1}). Hence, at the large scale, the data indicate a rather stable configuration of the valleys since the Middle Pleistocene. Other aspects of this thesis potentially highlight some knickpoints (regressive erosion) observed above the chalk bedrock along the valley bottom (i.e., near the Poses dam or in the Bassée area). These knickpoints could originate from the same continuous base level fall, which would have occurred during limited periods of MIS 2 or MIS 6.

In conclusion, this study highlights that a combined approach involving (i) ESR-OSL measurements, (ii) valley bottom geometry restitution and (iii) sediment storage within the

valley bottom is highly valuable to further understand Late Quaternary sediment transfer within the Seine River catchment.

A PDF of this thesis can be obtained by contacting the author: diana.chourio_camacho@sorbonne-universite.fr

Gwynlyn R. Buchanan

Infrared radiofluorescence dating: new insights into the (upper) dating limit, grain size and feldspar chemistry

July 2024

University of Tübingen, Department of Geosciences, Tübingen, Germany

Degree: Dr. rer. nat.
Supervisors: Prof. Dr. Sumiko Tsukamoto,
Prof. Dr. Kathryn E. Fitzsimmons

Accurate luminescence dating of feldspar has long been hampered by the effect of athermal signal loss (anomalous fading) when using luminescence dating techniques that make use of recombination centres. Infrared radiofluorescence (IR-RF) dating is a luminescence dating technique that makes use of the principal trap and is therefore theorised to not suffer from fading to a significant extent. Extensive laboratory investigations have been done to better constrain and exploit the IR-RF signal and mechanisms but remarkably few have applied the technique to large sequences of natural sediments with known age control. In this dissertation, the utility and effectiveness of IR-RF dating were investigated and tested on coarse-, mid- and polymineral fine-grains of feldspar with a view to evaluating the upper dating limit of IR-RF as well as compared IR-RF with the recently developed novel infrared photoluminescence (IRPL) dating technique. Initially ten coarse-grained K-feldspar samples (∼25 to ∼900 ka) from the Luochuan loess-paleosol sequence were measured and compared with age control and it was found that a bleaching time of 1,500 s (between the natural and regenerated measurements) underestimated across all but the youngest sample while a longer bleach of 20,000 s resulted in good agreement with the age control up to 300 ka (5 samples) and underestimated for the older samples. Construction of the natural and laboratory dose response curves across the sequence revealed significantly different curve shapes for the shorter bleaching time and consistent curve shapes for the longer bleaching time, highlighting the importance of the longer bleach time. The potential of the IR-RF signal for dating was then tested on six polymineral fine-grained samples, and it was observed that the IR-RF signal did not describe the characteristic decreasing stretched exponential curve shape; these results were compared with Na- and K-feldspar mid-grain fractions of the same samples. The essentially flat curves were attributed to the dominance of Na-feldspar and quartz in the polymineral fine grains. Despite the flat IR-RF signals and poor dose recoveries, the age results for the polymineral fine-grains were consistent with age control up to 300 ka, the Na-feldspar mid-grains up to 350 ka and the K-feldspar mid-grains up to 200 ka. A comparison of two IR-RF signals (at room temperature, RF_{RT}; and at 70 °C, RF_{70}) and two IRPL signals (stimulated at 880 nm, $IRPL_{880}$; and at 955 nm, $IRPL_{955}$) on four coarse-grained coastal sediments (∼133 to 223 ka) from Sardinia showed good agreement with age control for all signals within 2σ. The IR-RF signal is an effective dating tool up to 300 ka for coarse- and polymineral fine-grains and its performance is comparable with IRPL dating.

A PDF of this thesis can be obtained by contacting the author: gwynlyn.buchanan@uni-tuebingen.de

Neda Rahimzadeh

Towards extending the luminescence dating range of quartz: exploring the 375 °C quartz TL peak

July 2024

University of Tübingen, Department of Geosciences, Tübingen, Germany

Degree: Dr. rer. nat.
Supervisors: Prof. Dr. Sumiko Tsukamoto,
Prof. Dr. Kathryn E. Fitzsimmons

Optically stimulated luminescence (OSL) dating of quartz is widely used to establish an absolute chronology for Quaternary sedimentary deposits. However, its applicability is in general limited to the last ∼100–150 ka. Therefore, extending the range of quartz luminescence dating beyond this limitation is a key challenge. In the quest for extending this limit, other luminescence signals from quartz have been proposed, among which violet stimulated luminescence (VSL) is a promising signal. It is based on the use of violet stimulation (405 nm) to measure traps deeper than those accessible by blue light. The overall objective of this thesis is to develop and test the applicability of VSL dating to extend the quartz dating range. Attempts to establish an optimised single aliquot regenerative dose (SAR) protocol for VSL dating on four coarse-grained quartz samples from the coastal environment of Sardinia have not all been successful. It is found that the range of the applicability of the SAR VSL protocol is dependent on the natural dose size; using the SAR method for VSL dating remains challenging for samples with large natural doses (i.e., >250 Gy).

Subsequently, the multiple aliquot regenerative dose (MAR) protocol is, for the first time, tested on fine-grained quartz samples from a Chinese loess-palaeosol sequence in Luochuan with reference ages up to ∼1400 ka. The natural VSL dose response curve (DRC) saturates at about 900 Gy, which would potentially allow dating at the Luochuan section using VSL up to ∼300 ka. However, the application of the MAR protocol showed significant age underestimation for samples older than ∼100 ka. This MAR VSL age underestimation can clearly be attributed to the different shapes of natural and laboratory DRCs; the natural signal progressively deviates from the laboratory signal beyond ∼250 Gy. These observations are, however, contradicting the previous research in the same region, which showed that the MAR DRC using coarse-grained quartz samples from the Luochuan section can reproduce the shape of the natural DRC. It can therefore be concluded that the grain size plays an important role in obtaining reliable ages. A direct comparison of fine- (4–11 µm) and coarse-grained (63–100 µm) quartz VSL data from nine samples from a loess section in southern Germany further confirm these observations. It is shown that there is a systematic tendency for the fine-grained VSL ages towards underestimation with increasing age. The fine-grained MAR DRC starts to deviate from the natural DRC at ~300 Gy and therefore tends to underestimate the reference ages beyond ~100 ka. In addition to the VSL signal, the physical characteristics and applicability of the multiple aliquot methods (MAR and multiple aliquot additive dose, MAAD) of the quartz isothermal thermoluminescence (ITL) signal measured at 330 °C (ITL_{330}) is systematically investigated by using nine fine-grained quartz samples from the Luochuan section. The natural ITL_{330} shows that the signal has a theoretical dating range up to ~800 Gy, equivalent to ~230 ka. The comparison of the natural and laboratory DRCs using MAR and MAAD protocols indicates that they start to diverge in shape beyond ~200 Gy, setting an upper limit for reliable ITL_{330} dating of ~70 ka. However, application of pulsed-irradiation (PI) for the MAAD protocol reveals that the shape of the natural DRC can mostly be reproduced with the PI-MAAD protocol and thus it can provide reliable ages up to natural saturation at ~230 ka.

Based on the observations summarised in this doctoral thesis it can be concluded that the natural VSL and ITL_{330} signals have an extended growth, and the main limitation is the deviation between natural and laboratory generated DRCs beyond a certain dose, which caused a progressive age underestimation. Application of pulsed irradiation increases the reproduction of the extended VSL and ITL_{330} natural growth. While further investigations will be needed, it appears that this method can be a promising step forward in our attempts to extend the quartz luminescence dating age range.

A PDF of this thesis can be downloaded from: http://hdl.handle.net/10900/158729

Victoria Schwarz

Hydroclimate Change Reconstructed from Lake-Margin Lunettes around Gariwerd in South-Eastern Australia

July 2024

University of Tübingen, Department of Geosciences, Tübingen, Germany

Degree: Masters
Supervisors: Prof. Dr. Kathryn Fitzsimmons, Dr. Tobias Lauer

Hydroclimate, defined as the interconnection of hydrology and climate, is highly important to assess environmental change. Especially in drought-prone regions, variability in hydroclimate can trigger major changes in landscape stability and affect ecosystems and human settlements. The highly variable hydroclimate with great variations in spatial and temporal landscape response in south-eastern Australia highlights the need of an improvement in the coverage of geochronologic and paleoenvironmental studies focussing on the reconstruction of hydroclimatic conditions. Lunettes, as transverse shoreline dunes at lakes, are valuable paleoenvironmental archives at the edge of Australia's dryland, as their sediment characteristics are altered through the conditions present during deposition and they are geomorphic proxies for the extent of the past dryland margins. In contrast, the lake bed is no suitable archive due to deflation. Periodic lake drying and lake bed deflation would result in clay pellet deposition whereas clean beach sand indicates full lake conditions. In this study, the history of lake filling and drying is investigated based on the lunettes for three former lakes (Lake Toolondo, Bryans Swamp, Nekeeya) around the mountain range Gariwerd/Grampians Ranges in western Victoria, Australia. This area is chosen due to its proximity to the semi-arid margin and the possibility to investigate whether an orographic effect on hydroclimate around the mountain range is preserved in the lunette's record. Toolondo is located west, Bryans Swamp in a southern valley and Nekeeya east of Gariwerd/Grampians Ranges. Optically stimulated luminescence (OSL) dating is used to constrain ages for sedimentation phases. Sediment characteristics, such as grain size and element composition, derived through laser diffractometry and portable X-ray fluorescence (pXRF), are used as proxies for lake conditions. This study enables the identification of the hydroclimatic history preserved in lunettes around Gariwerd/Grampians Ranges. At Toolondo drying lake conditions are preserved from ~100–80 ka. A minor lake full phase with lunette deposition is recorded at ~55 ka at Toolondo and Nekeeya. This is followed by major continuous to persisting sandy lunette deposition from ~34–30 ka to 16 ka at all three lakes. Afterwards, minor full lake lunette deposition or partly reworking occurred at Toolondo and Bryans Swamp from ~11–10 ka and at all three lakes from ~7–5 ka and ~2.4–1.7 ka. More recent activity is dated to ~0.6 ka and <150 a at Toolondo and Nekeeya. The mostly continuous water availability at the lakes investigated highlights the importance of snow melt and vegetation response in mountainous regions during periods of generally higher aridity. Within this study, no evidence for an orographic effect of the mountain range Gariwerd/Grampians Ranges onto past lake hydrology could be found. Instead, latitudinal effects, the proximity to the mountain range and the catchment characteristics seem to have a greater effect on water availability within the studied lakes. The obtained results bring up the hypothesis of a "megalake" at Bryans Swamp through linkage with the adjacent Mahoney Swamp before 32 ka. This study improved the knowledge about spatial and temporal variability in hydroclimatic conditions and its landscape response and provides further evidence for more water availability during the extended Last Glacial Maximum (LGM) due to either decreased evaporation, increased rainfall or snow melt. The data can be used to guide future approaches to quantify climatic parameters in the past.

A PDF of this thesis can be obtained by contacting the author: victoria.schwarz@monash.edu

Natalie Tanski

Dynamics of Climate and Tectonics on Surface Processes and Their Sedimentary Archives in the Colorado Plateau and Basin and Range, USA and the Calabrian Forearc, Sicily

August 2024

Utah State University, Logan, United States of America

Degree: Ph.D.
Supervisors: Tammy Rittenour, Joel Pederson

Landscapes change over time in response to movements of the Earth's crust and the effects of climate. This dissertation examines how these factors shape different landscapes, focusing on erosion of river canyons in elevated plateaus, how the transport history in quartz sand may be encoded in its properties, and how a paleo-delta has formed in response to sea-level change and fault displacement. I use dating techniques, field methods, and topographic analyses to offer insight into erosional patterns and rates in different landscapes.

Rivers can take a long time to adjust to changes in boundary conditions, even after those changes have ceased. I studied the Colorado River incision history in the tectonically stable central Colorado Plateau of Utah, to understand the timing, spatial variability, and controls on canyon carving. The incision history and topography of the region show remarkable variability in erosion across the region and through time, with significant rapid incision of ∼250 m in the last 350 ka. Results suggest this rapid erosion is a signal derived from baselevel fall by the Colorado River in the Grand Canyon region 5 million years ago. This study shows that even without major tectonic or climate change, landscapes can still maintain complex erosion patterns.

Optically stimulated luminescence sensitivity is a new technique used to study Earth's surface processes. However, the geologic processes that induce a luminescence phenomenon in quartz are still unknown. I investigate the geologic controls on the luminescence sensitivity of quartz sand using rocks and modern and paleo-river sediments in a small mountainous catchment in northern Utah, USA. The results indicate that the luminescence phenomena in quartz is enhanced with the time spent at the Earth's surface as the sand grain weathers, erodes, and is transported along hillslopes to river systems.

The Pagliara fan-delta in northeastern Sicily provides a unique opportunity to study how coastal sediments stack through time in response to climate and sea-level change and tectonic history. Dating of the delta using luminescence techniques, reveals that the delta formed 300–220 ka ago when accommodation space was generated by sea-level fall and subsidence from fault movement. After this time, river and shore processes began to excavate the delta, indicating a shift from sediment accumulation in the delta to tectonic uplift. Despite the change in tectonic stress revealed in the delta stratigraphy, the uplift and erosion rates of the region have remained relatively constant over the past 300 ka.

A PDF of this thesis can be downloaded from: https://digitalcommons.usu.edu/etd2023/250/

Hawke Woznick

Shedding Light on Past Ice-Free Intervals in Northwest Greenland: Luminescence Dating of the Base of the Camp Century Ice Core

August 2024

Utah State University, Logan, United States of America

Degree: Masters
Supervisor: Tammy Rittenour

The goal of this thesis is to provide greater resolution on the sub-glacial sediment ages and duration of ice-free intervals recorded in the Camp Century ice core, northwestern Greenland. Bulk sediment geochemistry and mineralogy were used to determine differences in sediment source and weathering, feldspar types, and inform sample selection for luminescence dating, which provides an age estimate of the last time sediment was exposed to sunlight.

The Camp Century core is separated into five subglacial sediment units. Samples were collected from each unit except unit 2, which is primarily composed of silty ice. Analysis of the bulk sediment geochemistry indicated the uppermost sediments were most depleted of soluble cations, indicating either sorting during transport or greater weathering. Statistical t-tests of the differences in the major elements in the sediment units above and below the silty ice lens (Unit 2) indicate that the upper sediments (Units 5, 4, and 3) are chemically different than the lower sub-glacial unit (Unit 1). Analysis of feldspars within the very fine sand fraction from each unit indicate they are dominated by K-feldspar, with an internal K content of 12.5 %, the value assumed for luminescence calculations. Age control on Camp Century subice sediment was obtained using post-infrared stimulated luminescence on the very fine-grained feldspar sand fraction. Luminescence results from the basal sediment unit (Unit 1) indicated that it was beyond the range of dating (>1.5 Ma). Preliminary luminescence results for the upper sedimentary units returned ages between 414 ka and 422 ka. These results confirm the initial age from the upper 10 cm of the core and indicate that Camp Century was last ice-free during the exceptionally long and warm Marine Isotope Stage 11 interglacial. An ice-free Camp Century within the last 400 ka greatly changes our understanding of the history and stability of the Greenland ice sheet. This research reveals that the Greenland ice sheet is more susceptible to melting, leading to global sea-level rise, than previously assumed.

A PDF of this thesis can be downloaded from: https://digitalcommons.usu.edu/etd2023/281/

Philip Liebrecht

Sedimentology of lake-margin lunettes in the Corangamite region, southeastern Australia

September 2024

University of Tübingen, Department of Geosciences, Tübingen, Germany

Degree: Masters

Supervisors: Prof. Dr. Kathryn Fitzsimmons, Dr. Jan-Hendrik May

Research on past climatic and hydrologic conditions is of high relevance when faced with the challenges of anthropogenic climate change. With water as an essential factor, variability in hydroclimate can affect landscapes as well as human settlements to a high degree. Within the already highly hydro-climatically variable Australian continent we investigate sedimentary deposits including lunettes, commonly found on the down-wind side of ephemeral lakes, as well as aeolian and fluvial deposits. Especially lunettes are valuable palaeoenvironmental archives, with their sediment sequences recording hydrologic conditions in their basins during their deposition. Samples were taken from three lakes in the Western Plains of the Newer Volcanics Province in Victoria: Lake Corangamite, Beeac and Murdeduke. The area is characterised by complex morphologies including multiple volcanic eruption centers as well as huge sedimentary deposits, which resulted in the hypothesis that a Megalake had previously existed in the Western Plains basin. This as well as the episodic salinity, increasingly becoming a problem with the arrival of European settlers and their pastoral agriculture, makes the area highly interesting. Using a combination of Optically Stimulated Luminescence (OSL) dating, remote sensing and sediment analyses a palaeolake extent, albeit smaller than previously hypothesized, as well as cascadic overflow points were identified. At Lake Beeac, a depositional phase at ∼42 ka was identified, followed by two deposits during lake drying conditions at ∼33 ka and ∼28 ka, respectively, at Lake Murdeduke. Immediately pre-LGM (Last Glacial Maximum), aeolian deposition occurred at Lake Corangamite. After a long inactivity, deposition resumed at Lake Murdeduke during lake full conditions ∼5 ka, whereas aeolian deposition occurred once more at Lake Corangamite around 3.6 ka, indicating variability in the late Holocene. With the arrival of European settlers and onset of pastoralism, reactivation occurred at the sampling sites of Lake Murdeduke, with four samples dated at ∼200 a.

A PDF of this thesis can be obtained by contacting the author: philip.liebrecht@gmail.com

Emma T. Krolczyk

Using Luminescence Dating to Investigate Geomorphic and Archaeologic Features at the Wiggins Fork Bison Jump Complex, Northwestern Wyoming

December 2024

Utah State University, Logan, Utah, United States of America

Degree: Masters

Supervisor: Tammy M. Rittenour

The terraces of the Wiggins Fork River in northwestern Wyoming host thousands of cairns that form an extensive network of drivelines and at least seven jump funnels. These anthropogenically placed features comprise the Wiggins Fork Bison Jump Complex, used prehistorically by Native Americans as a hunting method where bison were driven off cliffs for harvest. Previous radiocarbon analysis from bison bones preserved at the base of Jump #4 indicated a ∼200-year duration of use, though the spatial distribution and varying degrees of cairn degradation across the complex suggest an extended utilization period. This thesis explores the use of luminescence dating to determine the construction ages of cairns associated with Jump #4 and provide the deposition age of geomorphic features associated with the hunting complex.

The terraces of the Wiggins Fork were mapped and dated, and the lowest Pleistocene terrace resulted in a luminescence age of 16–23 ka, indicating deposition during the Pinedale glaciation and correlation with the lowest Pleistocene terrace of the Wind River. Luminescence dating of the overlying fine-grained alluvial deposit indicated deposition at ∼11 ka, coinciding with the Pleistocene to Holocene climate transition, and provided a maximum age for the archaeological features associated with the complex. Luminescence dating of cairns associated with the funnel of Jump #4 indicated that the jump was constructed ∼300–800 years ago. These placement ages primarily fell within error of the radiocarbon ages associated with the jump and suggest that the jump funnel was constructed during or prior to successful utilization. Cairn mapping and luminescence dating revealed that four gully-dissected parallel drivelines extending along the terrace tread approaching Jump #4 were constructed between ∼300 and 800 years ago. Results from each of the parallel driveline suggest that the features may have been reconstructed further inland to accommodate headward gully migration and reinforce the previously constructed drivelines. This represents a long-term investment in the landscape and adaptation to geomorphic change. The coinciding luminescence ages and radiocarbon demonstrate that cairns at this site can be dated, removing the need to find and disrupt bone deposits from the other jumps. These results have implications for ongoing archaeological investigations and efforts to protect this culturally and historically valuable site.

A PDF of this thesis can be downloaded from: https://digitalcommons.usu.edu/etd/

Bibliography

Compiled by Sébastien Huot
From June 1, 2024 to December 1, 2024

<u>Various geological applications</u>

- aeolian

Cao, M., Lü, P., Ma, F., Yang, L., Yu, J., Xia, Z., Li, C., 2024. Holocene aeolian environmental dynamics in fixed and semi-fixed deserts over the arid Central Asia revealed by comprehensive sand-dune records. CATENA 246, 108368, http://doi.org/10.1016/j.catena.2024.108368

Carr, A.S., Hay, A.S., Bateman, M.D., Livingstone, I., Powell, D.M., 2024. How old are the Mojave topographic dunes? The implications of new luminescence dating analyses from the Cady Mountains, Mojave Desert, southwest USA. Geomorphology 463, 109349, http://doi.org/10.1016/j.geomorph.2024.109349

Liu, B., Ge, J., Li, S., Du, H., Liang, X., Jin, H., Jin, J., Zhao, H., Chen, F., 2024. Quantification of Middle to Late Holocene precipitation in the Gonghe Basin, northeastern Qinghai-Tibetan Plateau, from the geochemistry of aeolian surface soil. Quaternary Science Reviews 343, 108940, http://doi.org/10.1016/j.quascirev.2024.108940

Lukyanycheva, M.S., Kurbanov, R.N., Taratunina, N.A., Vasilieva, A.N., Lytkin, V.M., Panin, A.V., Anoikin, A.A., Stevens, T., Murray, A.S., Buylaert, J.-P., Knudsen, M.F., 2024. Dating post-LGM aeolian sedimentation and the Late Palaeolithic in Central Yakutia (northeastern Siberia). Quaternary Geochronology 83, 101563, http://doi.org/10.1016/j.quageo.2024.101563

Marković, R.S., Perić, Z.M., Gavrilov, M.B., Marković, S.B., Vandenberghe, J., Schaetzl, R.J., Obreht, I., Bartyik, T., Radaković, M.G., Radivojević, A., Marjanović, M., Lukić, T., Sipos, G., 2024. Aeolian dynamics at the northern edge of Deliblato (Banat) Sand Sea, Vojvodina, Serbia, at the time of the last deglaciation. Quaternary Research 121, 59-72, http://doi.org/10.1017/qua.2024.13

Maßon, L.A.E., Riedesel, S., Zander, A., Sontag-González, M., Reimann, T., 2024. Testing the applicability of standardised growth curves for chemically heterogeneous single-grain feldspars from the Atacama Desert, Chile. Quaternary Geochronology 83, 101585, http://doi.org/10.1016/j.quageo.2024.101585

Nowatzki, M., Fitzsimmons, K.E., Harder, H., Rosner, H.-J., 2024. Investigating palaeodune orientations and contemporary wind regimes in Southeast Kazakhstan using a semi-automated mapping framework. Earth Surface Processes and Landforms 49, 4553-4569, http://doi.org/10.1002/esp.5981

Yang, S., Liu, X., Zan, J., Li, P., Xu, X., Li, D., Li, Q., Liu, L., Wen, C., Fang, X., 2024. Multi-method luminescence dating of young aeolian dunes in the central Tibetan plateau. Quaternary Geochronology 83, 101595, http://doi.org/10.1016/j.quageo.2024.101595

- cave

Cao, Y., Zhang, X., Sun, X., Yu, L., Guo, X., Cai, H., Wang, X., 2024. OSL re-dating and paleoclimate of Laoya Cave in Guizhou Province, southwest China. Quaternary International 707, 50-59, http://doi.org/10.1016/j.quaint.2024.07.009

Hernando-Alonso, I., Moreno, D., Ortega, A.I., Benito-Calvo, A., Alonso, M.J., Campaña, I., Parés, J.M., Cáceres, I., García-Medrano, P., Carbonell, E., Bermúdez de Castro, J.M., 2024. ESR chronology of the endokarstic deposits of Galería complex (Sierra de Atapuerca, Spain). Quaternary Geochronology 83, 101575, http://doi.org/10.1016/j.quageo.2024.101575

Richard, M., Mercier, N., Weinstein-Evron, M., Weissbrod, L., Shimelmitz, R., 2024. Chronology of the late Lower and Middle Palaeolithic at Tabun Cave (Mount Carmel, Israel) with insights into diagenesis and dose rate variation using post-IR IRSL (pIRIR290) dating and infrared spectroscopy. Quaternary Geochronology 84, 101611, http://doi.org/10.1016/j.quageo.2024.101611

Stewart, M., Andrieux, E., Blinkhorn, J., Guagnin, M., Fernandes, R., Vanwezer, N., Hatton, A., Alqahtani, M., Zalmout, I., Clark-Wilson, R., Al-Mufarreh, Y.S.A., Al-Shanti, M., Zahrani, B., Al Omari, A., Al-Jibreen, F., Alsharekh, A.M., Scerri, E.M.L., Boivin, N., Petraglia, M.D., Groucutt, H.S., 2024. First evidence for human occupation of a lava tube in Arabia: The archaeology of Umm Jirsan Cave and its surroundings, northern Saudi Arabia. PLOS ONE 19, e0299292, http://doi.org/10.1371/journal.pone.0299292

Zhang, J., Klose, J., Scholz, D., Marwan, N., Breitenbach, S.F.M., Katzschmann, L., Kraemer, D., Tsukamoto, S., 2024. Isothermal thermoluminescence dating of speleothem growth – A case study from Bleßberg cave 2, Germany. Quaternary Geochronology 85, 101628, http://doi.org/10.1016/j.quageo.2024.101628

- coastal

Ben Arous, E., Bateman, M.D., Duval, M., 2024. Extending the ESR and OSL dating comparison on coastal dune deposits from the Wilderness-Knysna area (South Africa). Quaternary Geochronology 83, 101580, http://doi.org/10.1016/j.quageo.2024.101580

Bilbao-Lasa, P., Aranburu, A., Álvarez, I., del Val, M., Cheng, H., Arriolabengoa, M., Iriarte, E., 2023. Record of the last interglacial sea level highstand based on new coastal deposits in the Cantabrian margin (Northern Iberian Peninsula). Continental Shelf Research 266, 105096, http://doi.org/10.1016/j.csr.2023.105096

de Boer, A.-M., Seebregts, M., Wallinga, J., Chamberlain, E., 2024. A one-day experiment quantifying subaqueous bleaching of K-feldspar luminescence signals in the Wadden Sea, the Netherlands. Netherlands Journal of Geosciences 103, e22, http://doi.org/10.1017/njg.2024.18

Engel, M., Zander, A., Kehl, M., Feulner, G.R., Douglas, K., Al-Jahwari, N.S.A., Al-Hinai, N.H., Brückner, H., 2024. From the Northern Hajar Foothills to the Batinah Coast – a Geoarchaeological Survey at Saham and Dahwa (Northern Oman). Open Quaternary 10, 8, http://doi.org/10.5334/oq.141

Helm, C.W., Bateman, M.D., Carr, A.S., Cawthra, H.C., De Vynck, J.C., Dixon, M.G., Lockley, M.G., Stear, W., Venter, J.A., 2023. Pleistocene fossil snake traces on South Africa's Cape south coast. Ichnos 30, 98-114, http://doi.org/10.1080/10420940.2023.2250062

Kalińska, E., Weckwerth, P., Lamsters, K., Alexanderson, H., Martewicz, J., Rosentau, A., 2024. Paleostorm redeposition and post-glacial coastal chronology in the eastern Baltic Sea, Latvia. Geomorphology 467, 109456, http://doi.org/10.1016/j.geomorph.2024.109456

Kurbanov, R., Murray, A., Yanina, T., Buylaert, J.P., 2024. Dating the middle and late Quaternary Caspian Sea-level fluctuations: First luminescence data from the coast of Turkmenistan. Quaternary Geochronology 83, 101599, http://doi.org/10.1016/j.quageo.2024.101599

Laerosa, A., Pradit, S., Wattanavatee, K., Duerrast, H., Vichaidid, T., Luengchavanon, M., Noppradit, P., 2024. Coastal Evolution of Satingpra Peninsula, Songkhla Province: Implications for Understanding Songkla Lagoon Formation. Trends in Sciences 21, 7508, http://doi.org/10.48048/tis.2024.7508

Malkowski, M.A., Sickmann, Z.T., Fregoso, T., McKee, L., Stockli, D.F., Jaffe, B., 2024. Reversal in estuarine sand supply driven by Holocene sea level rise: A model for sand transport in large structural estuaries, San Francisco Bay, California, USA. Earth and Planetary Science Letters 643, 118887, http://doi.org/10.1016/j.epsl.2024.118887

Moreira, V.B., Lämmle, L., Torres, B.A., Donadio, C., Perez Filho, A., 2024. Geomorphological evolution in transitional environments on the eastern coast of Brazil. Earth Surface Processes and Landforms 49, 4679-4693, http://doi.org/10.1002/esp.5989

Prado, J.L., Duval, M., Demuro, M., Santos-Arévalo, F.J., Alberdi, M.T., Tomassini, R.L., Montalvo, C.I., Bonini, R., Favier-Dubois, C.M., Burrough, S., Bajkan, S., Gasparini, G.M., Bellinzoni, J., Fernández, F.J., García-Morato, S., Marin-Monfort, M.D., Adams, S., Zhao, J.-x., Beilinson, E., Fernández-Jalvo, Y., 2024. Refining the chronology of Middle/Late Pleistocene fossil assemblages in the Argentine Pampas. Quaternary Science Reviews 344, 108958, http://doi.org/10.1016/j.quascirev.2024.108958

Semikolennykh, D., 2024. Late Quaternary history of the Kerch Strait — the stratotype region for the Black Sea. Quaternary Science Reviews 342, 108914, http://doi.org/10.1016/j.quascirev.2024.108914

- colluvial

Ranulpho, R., Carlos de Barros Corrêa, A., Jorge de Lima, F., Paisani, J.C., 2024. Quaternary geomorphological dynamics of colluvial deposits from silicophytoliths and soil micromorphology, Araripe plateau, northeast of Brazil. Quaternary International 697, 1-18, http://doi.org/10.1016/j.quaint.2024.06.010

- earthquake (and fault related)

Bhadran, A., Duarah, B.P., Girishbai, D., Atif Raza, M., Mero, A., Lahon, S., A.L, A., Gopinath, G., 2024. Soft sediment deformation structures from the Brahmaputra Basin: A window to the eastern Himalayan paleoseismicity and tectonics. Journal of Asian Earth Sciences 259, 105894, http://doi.org/10.1016/j.jseaes.2023.105894

Forlin, P., Reicherter, K., Gerrard, C.M., Bailiff, I., García Porras, A., 2024. Recovering a lost seismic disaster. The destruction of El Castillejo and the discovery of the earliest historic earthquake affecting the Granada region (Spain). PLOS ONE 19, e0300549, http://doi.org/10.1371/journal.pone.0300549

Fougere, D., Dolan, J., Rhodes, E., McGill, S., 2024. Refined Holocene Slip Rate for the Western and Central Segments of the Garlock Fault: Record of Alternating Millennial-Scale Periods of Fast and Slow Fault Slip. Seismica 3, http://doi.org/10.26443/seismica.v3i2.1202

Heydari, M., Ghassemi, M.R., Grützner, C., Tsukamoto, S., Chruścińska, A., Preusser, F., 2024. First luminescence dating of exhumed fault-zone rocks of the North Tehran Fault, Iran. Quaternary Geochronology 83, 101562, http://doi.org/10.1016/j.quageo.2024.101562

Kaya, A., 2024. Paleoseismological trenching and seismic hazard assessment of the Bozkurt Segment of the Maymundağı Fault, Acıgöl Graben, SW Türkiye. Journal of Mountain Science 21, http://doi.org/10.1007/s11629-024-9027-8

Malik, J.N., Srivastava, E., Gadhavi, M.S., Livio, F., Sharma, N., Arora, S., Parrino, N., Burrato, P., Sulli, A., 2024. Holocene surface-rupturing paleo-earthquakes along the Kachchh Mainland Fault: shaping the seismic landscape of Kachchh, Western India. Scientific Reports 14, 11612, http://doi.org/10.1038/s41598-024-62086-z

Öncü, U., Sözbilir, H., Özkaymak, Ç., Softa, M., Sümer, Ö., Eski, S., Spencer, J.Q.G., Şahiner, E., Yüksel, M., Meriç, N., Topaksu, M., 2024. Palaeoseismological assessment for a seismic gap located very close to the epicentre of the 30 October 2020 Samos Earthquake (M6.9), western Anatolia, Turkey. Natural Hazards 120, 4699-4727, http://doi.org/10.1007/s11069-023-06290-6

Saha, U.D., Bhattacharya, H.N., Islam, A., 2024. Neotectonic impact on drainage development in the Eastern Himalayan foreland basin. Geomorphology 462, 109328, http://doi.org/10.1016/j.geomorph.2024.109328

Sharma, R., Singh, Y., Rajwant, Singh, N., Malik, J.N., Dhali, M., Srivastava, E., Sharma, N., 2024. Appraisal of Active Tectonics: An Insight from the Morphotectonic Study of Drainage Basins and OSL Dating in the Kangra Area, Himachal Pradesh. Journal of the Geological Society of India 100, 996-1006, http://doi.org/10.17491/jgsi/2024/173942

Tsodoulos, I.M., Gallousi, C., Stamoulis, K., Chatzipetros, A., Pavlides, S., Ioannides, K., 2024. Tectonic geomorphology and paleoseismology of the Angelochori fault segment of the Anthemountas extensional detachment fault, Central Macedonia, Greece: Paleoseismic evidence from the 1677 CE earthquake. Geomorphology 463, 109372, http://doi.org/10.1016/j.geomorph.2024.109372

Zinke, R., Dolan, J.F., Rhodes, E.J., Van Dissen, R.J., Hatem, A.E., McGuire, C.P., Brown, N.D., Grenader, J.R., 2021. Latest Pleistocene–Holocene Incremental Slip Rates of the Wairau Fault: Implications for Long-Distance and Long-Term Coordination of Faulting Between North and South Island, New Zealand. Geochemistry, Geophysics, Geosystems 22, e2021GC009656, http://doi.org/10.1029/2021GC009656

- fluvial

Abdulkarim, M., Schmitt, L., Fülling, A., Rambeau, C., Ertlen, D., Mueller, D., Chapkanski, S., Preusser, F., 2024. Late glacial to Holocene fluvial dynamics in the Upper Rhine alluvial plain, France. Quaternary Research 121, 109-131, http://doi.org/10.1017/qua.2024.22

Bartz, M., Duval, M., Alonso Escarza, M.J., Rixhon, G., 2024. Older than expected: fluvial aggradation of the Rhine's main terrace at Kärlich dated around 1.5 Ma by electron spin resonance. E&G Quaternary Science Journal 73, 139-144, http://doi.org/10.5194/egqsj-73-139-2024

Boterman, L., Candel, J., Makaske, B., Wallinga, J., 2024. Late-Holocene counterpoint deposition in the Lower Rhine River. Sedimentology 71, 1457-1476, http://doi.org/10.1111/sed.13180

Breda, C., Pupim, F.N., Cruz, C.B.L., Souza, P.E., Monsalve, G., Cardona, A., Sawakuchi, A.O., Parra, M., 2024. Variation in the ITCZ position controls the evolution of the piedmont landscape of the tropical Andes (Colombia) during the late Quaternary. Geomorphology 462, 109333, http://doi.org/10.1016/j.geomorph.2024.109333

Chauhan, V., Mandal, S.K., Scherler, D., Jaiswal, M.K., Christl, M., Shukla, A.D., 2024. Prolonged sediment aggradation in an internal Himalayan valley due to out-of-sequence lateral fault growth. Earth and Planetary Science Letters 647, 119054, http://doi.org/10.1016/j.epsl.2024.119054

Chourio-Camacho, D., Grimaud, J.-L., Tissoux, H., Bessin, P., Voinchet, P., Vartanian, E., Noble, M., Bertran, P., 2024. Incision and rock uplift along the Lower Seine River since Marine Isotope Stage 8. Journal of Quaternary Science 39, 872-889, http://doi.org/10.1002/jqs.3640

Cloete, G., Benito, G., Grodek, T., Porat, N., Hoffman, J., Enzel, Y., 2022. Palaeoflood records to assist in design of civil infrastructure in ephemeral rivers with scarce hydrological data: Ugab River, Namibia. Journal of Hydrology: Regional Studies 44, 101263, http://doi.org/10.1016/j.ejrh.2022.101263

Euzen, C., Chabaux, F., Rixhon, G., Preusser, F., Eyrolle, F., Chardon, V., Zander, A.M., Badariotti, D., Schmitt, L., 2024. Multi-method geochronological approach to reconstruct post-1800 floodplain sedimentation in the upper Rhine plain, France. Quaternary Geochronology 83, 101561, http://doi.org/10.1016/j.quageo.2024.101561

Huang, X., Zhang, Y., Guo, Y., Ge, Y., Mao, P., Liu, T., Wang, S., 2024. Outburst flood events since the Last Glacial Maximum in the Hutiao Gorge of Jinsha River: Geomorphological evidence from eddy gravel bars. Geomorphology 465, 109415, http://doi.org/10.1016/j.geomorph.2024.109415

Knight, J., Evans, M., 2024. Flood dynamics on the upper Letaba River, South Africa, deduced from luminescence dating. South African Geographical Journal 106, 423-445, http://doi.org/10.1080/03736245.2024.2333764

Layzell, A.L., Andrzejewski, K.A., Mandel, R.D., Hanson, P.R., 2024. Landscape and paleoenvironmental change in stream valleys of the Central Great Plains, North America, during Marine Isotope Stage 3 (ca. 59–27 ka). Quaternary Science Reviews 338, 108830, http://doi.org/10.1016/j.quascirev.2024.108830

Li, K., Qin, J., Chen, J., Liu, J., Yao, Y., 2024. Unraveling the deposition and incision paces of alluvial fan-river system by using single grain K-feldspar luminescence dating. Quaternary Geochronology 83, 101587, http://doi.org/10.1016/j.quageo.2024.101587

Li, Y., Sun, X., Liu, Y., Pei, Y., 2024. Timing of fluvial sedimentation in the Baiyangdian catchment, North China Plain, since the late Pleistocene by multiple luminescence dating approaches. Quaternary Geochronology 83, 101589, http://doi.org/10.1016/j.quageo.2024.101589

Liu, Q., Chen, J., Qin, J., Yang, H., Liu, J., Li, T., Di, N., Li, K., Pu, Y., Li, S., 2024. Incision rate of the Manas River, northern Tian Shan: Insight from luminescence dating of terrace cobbles. Quaternary Geochronology 83, 101593, http://doi.org/10.1016/j.quageo.2024.101593

Lyons, R., Tooth, S., Duller, G.A.T., McCarthy, T., 2024. Are human activities or climate changes the main causes of soil erosion in the South African drylands?: A palaeo-perspective from three sites in the interior. Journal of Quaternary Science 39, 1116-1137, http://doi.org/10.1002/jqs.3651

Ma, Q.-H., Guo, Y.-J., Lei, H.-R., Shen, Y.-H., Wang, J.-J., Liu, Y., Zhou, Z.-Y., Zhang, J.-F., 2024. Holocene paleoenvironment of the Nihewan Basin, China, inferred from high-resolution luminescence dating and a multiproxy analysis of gully sediments. Palaeogeography, Palaeoclimatology, Palaeoecology 655, 112533, http://doi.org/10.1016/j.palaeo.2024.112533

Magyar, G., Bartyik, T., Marković, R.S., Filyó, D., Kiss, T., Marković, S.B., Homolya, V., Balla, A., Bozsó, G., Baranya, S., Alexanderson, H., Lukić, T., Sipos, G., 2024. Downstream change of luminescence sensitivity in sedimentary quartz and the rearrangement of optically stimulated luminescence (OSL) components along two large rivers. Quaternary Geochronology 85, 101629, http://doi.org/10.1016/j.quageo.2024.101629

Makeev, A., Rusakov, A., Lebedeva, M., Karpukhina, N., Konstantinov, E., Frechen, M., Kust, P., 2024. Unveiling the enigma of the Upper Volga River valley based on the soilscape studies. CATENA 246, 108431, http://doi.org/10.1016/j.catena.2024.108431

Panda, S., Kumar, A., Srivastava, P., Das, S., Jayangondaperumal, R., Prakash, K., 2022. Deciphering the role of late Quaternary sea level fluctuations in controlling the sedimentation in the Brahmaputra Plains. Sedimentary Geology 442, 106289, http://doi.org/10.1016/j.sedgeo.2022.106289

Pederson, J.L., Young, S.C., Turley, M., Tanski, N., Rittenour, T.M., Harris, R.A., 2024. The how, when, and why of an abandoned bedrock meander of the Colorado River, Utah (U.S.). Earth Surface Processes and Landforms 49, 3283-3291, http://doi.org/10.1002/esp.5886

Prokešová, R., Danišík, M., Fiebig, M., Jourdan, F., Lüthgens, C., Procházka, J., Holec, J., Minár, J., 2024. Late Cenozoic alkali basalts and their interactions with the paleo-Hron River (Western Carpathians): New insights from geochronology and fluvial morphometric indices. Geomorphology 463, 109326, http://doi.org/10.1016/j.geomorph.2024.109326

Rahimzadeh, N., Hein, M., Urban, B., Weiss, M., Tanner, D.C., Khosravichenar, A., Tsukamoto, S., Lauer, T., 2024. Dating the Neanderthal environment: Detailed luminescence chronology of a palaeochannel sediment core at the Palaeolithic site of Lichtenberg in the Lower Saxony, northern Germany. Quaternary Geochronology 83, 101564, http://doi.org/10.1016/j.quageo.2024.101564

Schwendel, A.C., Milan, D.J., Pope, R.J.J., Williams, R., Thompson, W., 2024. Using geophysical subsurface data for the reconstruction of valley-scale spatio-temporal floodplain evolution: Implications for upland river restoration. Geomorphology 466, 109459, http://doi.org/10.1016/j.geomorph.2024.109459

Seeger, K., May, S.M., Brill, D., Herbrecht, M., Hoffmeister, D., Quandt, D., Stoll, A., Rhein, A., Keiser, M., Wolf, D., Bubenzer, O., 2024. Geomorphological and sedimentary traces of historical and modern exceptional flooding events in a dry valley of the Andean Precordillera (Tarapacá Region, N Chile). Geomorphology 466, 109417, http://doi.org/10.1016/j.geomorph.2024.109417

Shen, Q., Feng, X., Zhou, Y., Lin, P., Liu, Y., Lai, Y., Han, J., Liu, Y., Wang, Y., Zhu, S., Li, Z., Lai, Z., 2024. Sedimentation history linked to global change in the alpine Damqu Wetland of the Yangtze River headwater in interior Tibetan Plateau. Quaternary Geochronology 83, 101598, http://doi.org/10.1016/j.quageo.2024.101598

Shivsagar, V., Basumatary, D., Goswami, C., Rawat, M., Singh, S., Jaiswal, M.K., 2024. An assessment of oxbow lakes and their potential in reconstructing past river discharge: Implication to reconstruct past climate in Southern West Bengal. Geochronometria 51, 192455, http://doi.org/10.20858/geochr/192455

Souza, A.d.O., Filho, A.P., Arruda, E.M., Cerrone, C., Lämmle, L., 2024. Fluvial responses to Holocene climatically induced coastline migration in the Iguape River estuary (Southeast Brazil). Earth Surface Processes and Landforms 49, 4694-4708, http://doi.org/10.1002/esp.5990

Steelquist, A.T., Seixas, G.B., Gillam, M.L., Saha, S., Moon, S., Hilley, G.E., 2024. The impact of bedrock meander cutoffs on 50 kyr scale incision rates, San Juan River, Utah. Earth Surface Dynamics 12, 1071-1089, http://doi.org/10.5194/esurf-12-1071-2024

Szymak, A., Moska, P., Sokołowski, R.J., Poręba, G., Tudyka, K., 2024. Chronostratigraphy of the Late Glacial Żabinko site (western Poland) and investigation of the dose rate variability. Geochronometria 51, 189750, http://doi.org/10.20858/geochr/189750

Tooth, S., Keen-Zebert, A., Grenfell, M.C., Addison, G., 2024. Timescales of tree-covered island dynamics on the mixed bedrock-alluvial anabranching Vaal River, South Africa. River Research and Applications 40, 1049-1066, http://doi.org/10.1002/rra.4296

Vasilieva, A.N., Murray, A.S., Taratunina, N.A., Buylaert, J.-P., Lytkin, V.M., Shaposhnikov, G.I., Stevens, T., Ujvari, G., Kertész, T.G., Kurbanov, R.N., 2024. Absolute dating of sediments forming the Lena river terraces (Northeastern Siberia). Quaternary Geochronology 83, 101592, http://doi.org/10.1016/j.quageo.2024.101592

Yu, Y., Wang, X., Yang, X., Yi, S., Lu, H., 2024. Diverse fluvial aggradation and incision response to interglacial—Glacial transitions in the headwaters of the Yangtze River, SE Tibetan Plateau. Geomorphology 465, 109418, http://doi.org/10.1016/j.geomorph.2024.109418

Zhao, Y., Fan, N., Nie, J., Abell, J.T., An, Y., Jin, Z., Wang, C., Zhang, J., Liu, X., Nie, R., 2023. From Desiccation to Re-Integration of the Yellow River Since the Last Glaciation. Geophysical Research Letters 50, e2023GL103632, http://doi.org/10.1029/2023GL103632

Zhong, Y., Picotti, V., Xiong, J., Willett, S.D., Schmidt, C., King, G., 2024. New data on tributary terraces and a reappraisal of the incision history of the Jinshan Gorge, middle Yellow River. Geomorphology 462, 109330, http://doi.org/10.1016/j.geomorph.2024.109330

- glacial and periglacial

Alexanderson, H., Lund, E.M., Bjermo, T., 2024. From ice-dammed lake to aeolian dunes in the Store Mosse area, SW Sweden. Quaternary Geochronology 83, 101591, http://doi.org/10.1016/j.quageo.2024.101591

Bhardwaj, P., Nagar, Y.C., Singh, T., Shekhar, M.S., Ganju, A., 2024. Reconstruction of landscape change of Shyok valley, Ladakh during Late Quaternary using OSL technique. Quaternary International 710, 1-17, http://doi.org/10.1016/j.quaint.2024.08.010

Buechi, M.W., Landgraf, A., Madritsch, H., Mueller, D., Knipping, M., Nyffenegger, F., Preusser, F., Schaller, S., Schnellmann, M., Deplazes, G., 2024. Terminal glacial overdeepenings: Patterns of erosion, infilling and new constraints on the glaciation history of Northern Switzerland. Quaternary Science Reviews 344, 108970, http://doi.org/10.1016/j.quascirev.2024.108970

Campos, M.C., Chiessi, C.M., Nascimento, R.A., Kraft, L., Radionovskaya, S., Skinner, L., Dias, B.B., Pinho, T.M.L., Kochhann, M.V.L., Crivellari, S., Mineli, T.D., Mendes, V.R., Baker, P.A., Silva, C.G., Sawakuchi, A.O., 2025. Millennial- to centennial-scale Atlantic ITCZ swings during the penultimate deglaciation. Quaternary Science Reviews 348, 109095, http://doi.org/10.1016/j.quascirev.2024.109095

Cheng, L., Long, H., Zhang, J., Wu, Y., Cheng, J., Yang, L., Cheng, H., 2024. Retreating ice sheet caused a transition from cold-dry to cold-humid conditions in arid Central Asia. Quaternary Science Reviews 345, 109057, http://doi.org/10.1016/j.quascirev.2024.109057

Efimova, M.O., Deev, E.V., Taratunina, N.A., Buylaert, J.P., Sosin, P.M., Panin, A.V., Murray, A.S., Schneider, R., Lukyanycheva, M.S., Tokareva, O.A., Meshcheryakova, O.A., Kurbanov, R.N., 2024. Luminescence dating of the MIS 6 glaciation of the Pamir mountains (Central Asia). Quaternary Geochronology 83, 101596, http://doi.org/10.1016/j.quageo.2024.101596

Firla, G., Lüthgens, C., Neuhuber, S., Schmalfuss, C., Kroemer, E., Preusser, F., Fiebig, M., 2024. Analyzing complex single grain feldspar equivalent dose distributions for luminescence dating of glacially derived sediments. Quaternary Geochronology 85, 101627, http://doi.org/10.1016/j.quageo.2024.101627

Kirsten, F., Starke, J., Bauriegel, A., Müller, R., Jouaux, J., Lüthgens, C., Sinapius, R., Hardt, J., 2024. Age, composition and spatial distribution of sandy loess in north-eastern Germany (Fläming, Brandenburg). Earth Surface Processes and Landforms 49, 3261-3282, http://doi.org/10.1002/esp.5885

Prince, K.K., Briner, J.P., Walcott, C.K., Chase, B.M., Kozlowski, A.L., Rittenour, T.M., Yang, E.P., 2024. New age constraints reveal moraine stabilization thousands of years after deposition during the last deglaciation of western New York, USA. Geochronology 6, 409-427, http://doi.org/10.5194/gchron-6-409-2024

Ruchkin, M.V., Nosevich, E.S., Sheetov, M.V., Brill, D., 2024. Stratigraphy and OSL chronology of the Middle–Upper Pleistocene sedimentary sequence and vegetation history during Late MIS6–MIS5e in the Neva Lowland (St. Petersburg region, Russia). Journal of Quaternary Science 39, 745-764, http://doi.org/10.1002/jqs.3618

Sechi, D., Stevens, T., Hällberg, P., Smittenberg, R.H., Molnár, M., Kertész, G.T., Buylaert, J.P., Schneider, R., Edward, C., Rasmussen, K.R., Knudsen, N.A.T., Andreucci, S., Pascucci, V., 2024. High resolution luminescence and radiocarbon dating of Holocene Aeolian silt (loess) in west Greenland. Quaternary Geochronology 84, 101579, http://doi.org/10.1016/j.quageo.2024.101579

Utkina, A., Choi, J.-H., Murray, A., Panin, A., Zaretskaya, N., Kurbanov, R., Buylaert, J.-P., 2024. Luminescence ages of sediments from the margin of the penultimate glaciation in the north-eastern East European plain. Quaternary Geochronology 83, 101578, http://doi.org/10.1016/j.quageo.2024.101578

Xu, Y., Ou, X., Zou, X., Yang, C., Duller, G.A.T., Li, Y., Roberts, H.M., Yang, K., Zeng, L., 2024. Single-grain K-feldspar post-IR IRSL dating of glaciofluvial sediments of Guxiang Glaciation in SE Tibetan Plateau. Quaternary Geochronology 84, 101612, http://doi.org/10.1016/j.quageo.2024.101612

Yang, J., Wang, Y., Li, G., Wang, X., Lu, T., Ding, W., Ou, X., Gao, D., 2024. Single grain pIRIR dating of glacigenic deposits in the Yuzhu Peak area of Kunlun Mountains of Tibetan Plateau revealed the glaciations during Holocene period. Quaternary Geochronology 83, 101586, http://doi.org/10.1016/j.quageo.2024.101586

- lacustrine

Hou, Y., Long, H., Zhang, J., Dai, G., Zhang, Z., 2024. Asynchronous hydroclimate changes across the Tibetan Plateau during Marine Isotope Stage 5. Quaternary Science Reviews 344, 108931, http://doi.org/10.1016/j.quascirev.2024.108931

Hu, F., Xiao, X., Fan, Q., Yu, L., Xu, Y., Feng, Y., Zhou, Y., Yu, M., 2025. Grain size and shape analysis of recent and paleo sediments along Poyang Lake with insight into its environmental significance. CATENA 248, 108588, http://doi.org/10.1016/j.catena.2024.108588

Polymeris, G.S., Geraga, M., Papatheodorou, G., Iliopoulos, I., Pluháček, T., Lemr, K., Qin, Z., Sergiou, S., Dimas, X., Liritzis, I., 2024. Climate-driven versus anthropogenic induced erosion of the last 3000 years from an ancient lake in the Southern Phokis Plain (Desfina), Greece. The Holocene 34, 1775-1789, http://doi.org/10.1177/09596836241275024

Schaller, S., Böttcher, M.E., Buechi, M.W., Epp, L.S., Fabbri, S.C., Gribenski, N., Harms, U., Krastel, S., Liebezeit, A., Lindhorst, K., Marxen, H., Raschke, U., Schleheck, D., Schmiedinger, I., Schwalb, A., Vogel, H., Wessels, M., Anselmetti, F.S., 2022. Postglacial evolution of Lake Constance: sedimentological and geochemical evidence from a deep-basin sediment core. Swiss Journal of Geosciences 115, 7, http://doi.org/10.1186/s00015-022-00412-1

Staff, R.A., Sanderson, D.C.W., Rex, C.L., Cresswell, A., Hyodo, M., Kitaba, I., Marshall, M.H., Schlolaut, G., Yamada, K., Suzuki, Y., Nowinski, V., Tada, R., Nakagawa, T., 2024. A luminescence-derived cryptostratigraphy from the Lake Suigetsu sedimentary profile, Japan: 45,000–30,200 IntCal20 yr BP. Quaternary Geochronology 83, 101588, http://doi.org/10.1016/j.quageo.2024.101588

Wang, X., Li, G., Yang, H., Wang, Y., Jin, M., Yan, Z., Qin, C., Gou, S., Pan, L., Yang, J., 2024. Single-grain luminescence dating of Manas Lake paleoshorelines reveals late quaternary glacial meltwater forced lake level highstand in arid Central Asia. Quaternary Geochronology 83, 101601, http://doi.org/10.1016/j.quageo.2024.101601

Zhang, J., Cao, X., Zhang, Z., He, M., Kong, X., Zhao, Z., 2024. The post-IR IRSL dating of an ancient dammed lake upstream of the Ganglai gorge in the upper-middle reaches of Yarlung Tsangpo. Quaternary Geochronology 83, 101570, http://doi.org/10.1016/j.quageo.2024.101570

Zhang, S., Zhao, H., Wang, L., Chen, F., 2024. Holocene lake shrinkage on the northwestern Tibetan Plateau revealed by K-feldspar single-grain pIRIR dating of paleo-shorelines. Quaternary Geochronology 83, 101583, http://doi.org/10.1016/j.quageo.2024.101583

- loess

Challier, A., Thomsen, K.J., Kurbanov, R., Sosin, P., Murray, A., Guérin, G., Meshcheryakova, O., Karayev, A., Khormali, F., Taratunina, N., Utkina, A., Buylaert, J.-P., 2024. A detailed quartz and feldspar luminescence chronology for the Khonako II loess section (Southern Tajikistan). Quaternary Geochronology 83, 101571, http://doi.org/10.1016/j.quageo.2024.101571

Gild-Haselwarter, C., Meyer, M., Geitner, C., Haas, J.N., Vranjes-Wessely, S., Hejny, C., Kofler, W., Krainer, K., Remias, D., Szidat, S., Sanders, D., 2024. Dynamic landscape response to Younger Dryas and earliest Holocene cooling events in the European Eastern Alps (Austria). Quaternary Science Reviews 344, 108959, http://doi.org/10.1016/j.quascirev.2024.108959

Kang, S., Huang, H., Wang, X., 2024. Luminescence dating of sandy loess along the middle Yellow River and its implications for aeolian–fluvial interactions. Quaternary Geochronology 83, 101584, http://doi.org/10.1016/j.quageo.2024.101584

Kehl, M., Seeger, K., Pötter, S., Schulte, P., Klasen, N., Zickel, M., Pastoors, A., Claßen, E., 2024. Loess formation and chronology at the Palaeolithic key site Rheindahlen, Lower Rhine Embayment, Germany. E&G Quaternary Science Journal 73, 41-67, http://doi.org/10.5194/egqsj-73-41-2024

Li, P., Yang, S., Luo, Y., Liu, L., Zhang, Y., Liu, W., Zhang, J., Xu, X., Wen, C., Li, Q., 2025. Indian summer monsoon history during the last glacial cycle revealed by a loess sequence from the Tibetan Plateau. Palaeogeography, Palaeoclimatology, Palaeoecology 657, 112593, http://doi.org/10.1016/j.palaeo.2024.112593

Perić, Z.M., Ryan, C., Alexanderson, H., Marković, S.B., 2024. Revised OSL chronology of the Kisiljevo loess-palaeosol sequence: New insight into the dust flux in the eastern Carpathian Basin during MIS 3 - MIS1. Quaternary International 698, 39-48, http://doi.org/10.1016/j.quaint.2024.06.006

Perić, Z.M., Stevens, T., Obreht, I., Hambach, U., Lehmkuhl, F., Marković, S.B., 2022. Detailed luminescence dating of dust mass accumulation rates over the last two glacial-interglacial cycles from the Irig loess-palaeosol sequence, Carpathian Basin. Global and Planetary Change 215, 103895, http://doi.org/10.1016/j.gloplacha.2022.103895

Zhao, H., Zhou, X., Yang, L., Long, H., Cheng, L., Yan, Y., Zhou, J., Sun, Q., Delang, C.O., He, H., 2024. Reconstructing the late Quaternary soil erosion and dust deposition dynamics in the southern Loess Plateau: Insights from Lake Luyanghu sedimentary records. Quaternary Science Reviews 346, 109000, http://doi.org/10.1016/j.quascirev.2024.109000

Zhao, Q., Peng, S., Liu, X., Ding, M., Wang, L., Hao, Q., Kang, S., Zhang, W., Xiong, R., Yue, J., Fan, T., 2024. Multi-step post-IR IRSL dating and palaeoclimate implications from 270 to 90 ka in the Central Shandong Mountains, eastern China. Quaternary Geochronology 83, 101590, http://doi.org/10.1016/j.quageo.2024.101590

- marine

Wang, Z., Tang, N., Lin, P., Qiao, P., Lu, K., Mei, X., Sun, J., Qi, J., Wang, Y., Chu, H., Lai, Z., 2024. OSL and radiocarbon dating of core TBF-1 on the outer shelf of the East China Sea and implications for late Quaternary stratigraphic correlation. Quaternary Geochronology 84, 101614, http://doi.org/10.1016/j.quageo.2024.101614

Xiong, W., Huang, L., Zhang, Y., Wang, Z., Bi, N.S., Pan, J., Sun, J., He, L., Wang, F., Mei, X., 2025. Quaternary transgression process controlled by tectonic subsidence over the last 1.35 Ma: New insights from the eastern Bohai Sea. Palaeogeography, Palaeoclimatology, Palaeoecology 657, 112602, http://doi.org/10.1016/j.palaeo.2024.112602

- soil

Chen, P., Lu, P., Tian, Y., Li, Y., Wang, H., Zhang, J., Zhao, X., Mo, D., 2024. The interplay between prehistoric vegetation, climatic fluctuations and anthropogenic activities in Central China. CATENA 247, 108540, http://doi.org/10.1016/j.catena.2024.108540

Choi, J., van Beek, R., Chamberlain, E.L., Reimann, T., Smeenge, H., van Oorschot, A., Wallinga, J., 2024. Luminescence dating approaches to reconstruct the formation of plaggic anthrosols. SOIL 10, 567-586, http://doi.org/10.5194/soil-10-567-2024

Duszyński, F., Waroszewski, J., Fenn, K., Kacprzak, A., Jancewicz, K., Egli, M., 2024. Cliff-foot sandy cones: A proxy to study the time frames, patterns and rates of sandstone caprock decay? CATENA 247, 108529, http://doi.org/10.1016/j.catena.2024.108529

Zhang, A., Long, H., Yang, F., Zhang, J., Peng, J., Gong, K., Hong, Y., Shi, Y., Zhou, S., Shao, Z., Yang, N., Huang, X., Luo, X., Zhang, G., 2025. Revisiting krotovina formation using luminescence dating − a case study from NE China. CATENA 248, 108554, http://doi.org/10.1016/j.catena.2024.108554

- surface exposure dating

Ageby, L., Jakathamani, S., Murray, A.S., Jain, M., Rades, E.F., 2024. Feasibility of rock surface luminescence dating technique for measuring the burial ages of unheated flints. Quaternary Geochronology 83, 101566, http://doi.org/10.1016/j.quageo.2024.101566

al Khasawneh, S., Murray, A., Thompson, W., 2024. Investigating luminescence-depth profiles from rocks with different lithologies. Radiation Measurements 176, 107192, http://doi.org/10.1016/j.radmeas.2024.107192

Andričević, P., Kook, M., Jain, M., 2024. Potential of luminescence imaging for screening sensitive and well-bleached samples for rock surface luminescence dating. Radiation Measurements 176, 107193, http://doi.org/10.1016/j.radmeas.2024.107193

Bailiff, I.K., Andrieux, E., Díaz-Guardamino, M., Alves, L.B., Comendador Rey, B., García Sanjuán, L., Martín Seijo, M., 2024. Dating the setting of a late prehistoric statue-menhir at Cruz de Cepos, NE Portugal. Quaternary Geochronology 83, 101569, http://doi.org/10.1016/j.quageo.2024.101569

Bench, T., Sanderson, D., Feathers, J., 2024. Observing impacts on luminescence depth profile evolutions from surface altered quartzite using OSL laser scanning and controlled light exposed rock sampling techniques. Quaternary Geochronology 83, 101600, http://doi.org/10.1016/j.quageo.2024.101600

Biswas, R.H., Pathan, A.N., Malik, J.N., 2023. General order kinetics model for OSL rock surface exposure dating. Proceedings of the Indian National Science Academy 89, 644-654, http://doi.org/10.1007/s43538-023-00172-y

Cossu, G., Sechi, D., Sohbati, R., Murray, A., Pascucci, V., Andreucci, S., 2024. Luminescence dating of rock surfaces in challenging environments: The case of MIS5e gravelly transgressive lag deposit (Southern Sardinia, West Mediterranean Sea). Quaternary Geochronology 85, 101630, http://doi.org/10.1016/j.quageo.2024.101630

Gliganic, L.A., McDonald, J., Mather, C., White, L.T., 2024. A method to date rock engravings using luminescence – tested at Murujuga, Western Australia. Quaternary Geochronology 85, 101633, http://doi.org/10.1016/j.quageo.2024.101633

Liu, Q., Chen, J., Qin, J., Yang, H., Liu, J., Li, T., Di, N., Li, K., Pu, Y., Li, S., 2024. Incision rate of the Manas River, northern Tian Shan: Insight from luminescence dating of terrace cobbles. Quaternary Geochronology 83, 101593, http://doi.org/10.1016/j.quageo.2024.101593

Pathan, A.N., Biswas, R.H., Lehmann, B., King, G.E., Herman, F., 2024. Towards accurate modelling of rock surface exposure dating using luminescence to estimate post-exposure erosion rate. Quaternary Geochronology 85, 101634, http://doi.org/10.1016/j.quageo.2024.101634

- tephra (and volcanic related)

Ji, H., Liu, C.-R., Li, W.-P., Wei, C.-Y., Neupane, B., Yin, G.-M., 2024. Evaluating signal bleaching of Al and Ti–Li centers in fluvio-lacustrine sediments of Datong, North China, and its implications for the volcanic eruption chronology. Quaternary Geochronology 83, 101568, http://doi.org/10.1016/j.quageo.2024.101568

Sontag-González, M., Li, B., O'Gorman, K., Burhan, B., Hakim, B., Brumm, A., Roberts, R.G., 2024. Survival of the brightest? pIRIR dating of volcanic sediments in Sulawesi, Indonesia, using micro-aliquots of K-rich feldspar. Quaternary Geochronology 85, 101638, http://doi.org/10.1016/j.quageo.2024.101638

Zolitschka, B., Preusser, F., Zhang, J., Hogrefe, I., Froitzheim, N., Böning, P., Schläfli, P., Bittmann, F., Binot, F., Frechen, M., 2024. Stratigraphy and dating of Middle Pleistocene sediments from Rodderberg, Germany. Journal of Quaternary Science 39, 1011-1030, http://doi.org/10.1002/jqs.3654

- thermochronology

Bartz, M., King, G.E., Bernard, M., Herman, F., Wen, X., Sueoka, S., Tsukamoto, S., Braun, J., Tagami, T., 2024. The impact of climate on relief in the northern Japanese Alps within the past 1 Myr–The case of the Tateyama mountains. Earth and Planetary Science Letters 644, 118830, http://doi.org/10.1016/j.epsl.2024.118830

Bouscary, C., King, G.E., 2024. Exploring the use of averaged thermal kinetic parameters in luminescence thermochronometry. Radiation Measurements 176, 107215, http://doi.org/10.1016/j.radmeas.2024.107215

Archaeology applications

Alfaro-Ibáñez, M.P., Cuenca-Bescós, G., Gómez-Olivencia, A., Demuro, M., Arnold, L.J., Arsuaga, J.L., 2024. Arvicolinae rodents of Galería de las Estatuas (Sierra de Atapuerca, Burgos) and insights into MIS 5- to −4 climatic conditions in Northern Iberia. Quaternary Science Reviews 343, 108939, http://doi.org/10.1016/j.quascirev.2024.108939

Arnold, L.J., Demuro, M., Duval, M., Grün, R., Sanz, M., Costa, A.M., Araújo, A.C., Daura, J., 2024. Single-grain luminescence and combined U-series/ESR dating of the early Upper Palaeolithic Lagar Velho Rock Shelter, Leiria, Portugal. Quaternary Geochronology 83, 101572, http://doi.org/10.1016/j.quageo.2024.101572

Bailiff, I.K., Andrieux, E., Díaz-Guardamino, M., Alves, L.B., Comendador Rey, B., García Sanjuán, L., Martín Seijo, M., 2024. Dating the setting of a late prehistoric statue-menhir at Cruz de Cepos, NE Portugal. Quaternary Geochronology 83, 101569, http://doi.org/10.1016/j.quageo.2024.101569

Ben Arous, E., Niang, K., Blinkhorn, J.A., Del Val, M., Medialdea, A., Coussot, C., Alonso Escarza, M.J., Bateman, M.D., Churruca Clemente, A., Blackwood, A.F., Iglesias-Cibanal, J., Saíz, C., Scerri, E.M.L., Duval, M., 2024. Constraining the age of the Middle Stone Age locality of Bargny (Senegal) through a combined OSL-ESR dating approach. Quaternary Environments and Humans 2, 100044, http://doi.org/10.1016/j.qeh.2024.100044

Beyin, A., Ryano, K.P., Buylaert, J.-P., Wright, D.K., 2025. Late Quaternary human occupation of the Kilwa coast (Tanzania): OSL ages and paleoenvironmental proxies from isotope geochemistry. Journal of Archaeological Science: Reports 61, 104874, http://doi.org/10.1016/j.jasrep.2024.104874

Castanet, C., Fernandes, A., Mokadem, F., Hatté, C., Gauthier, C., Develle-Vincent, A.-L., Cavero, J., Dru, H., Virmoux, C., Sipos, G., Dussol, L., Nondédéo, P., 2024. Wetland landscapes in the Southern Maya Lowlands (Naachtun, Guatemala) from the ancient agroecosystems to the tropical biosphere reserve: Ecology, exploitation and management of water and soil resources, and heritage legacy. Geoarchaeology 39, 530-562, http://doi.org/10.1002/gea.22003

Crassard, R., Abu-Azizeh, W., Barge, O., Brochier, J.É., Preusser, F., Seba, H., Kiouche, A.E., Régagnon, E., Sánchez Priego, J.A., Almalki, T., Tarawneh, M., 2023. The oldest plans to scale of humanmade mega-structures. PLOS ONE 18, e0277927, http://doi.org/10.1371/journal.pone.0277927

Demuro, M., Arnold, L.J., Duval, M., Churruca Clemente, A., Santonja, M., Pérez-González, A., 2024. Extended-range luminescence and ESR dating of Iberian fluvial terraces (Duero and Guadiana basins) associated with the Lower Palaeolithic sites of La Maya I, II, III, Burganes and Albalá (west-central Spain). Quaternary Geochronology 83, 101567, http://doi.org/10.1016/j.quageo.2024.101567

Di, N., Yang, H., Chen, J., Yang, J., Li, Y., Qin, J., Luo, M., 2024. Chronology of late Holocene sediments related to the Qicheng ruins in central China. Quaternary International 698, 1-10, http://doi.org/10.1016/j.quaint.2024.05.005

Ghasidian, E., Frouin, M., Grandfield, T., Hariri, N., Douka, K., Ashari, S., Samei, S., Kehl, M., Deckers, K., Azizi, F., Asiabani, S., Fotuhi, E., Ahmadnejad, F., Hariryan, H., Ramzanpour, H., Guran, S.H., 2024. Initial upper Palaeolithic on the Iranian Plateau: Sorheh Rockshelter, Southern Alborz mountains. Quaternary Science Reviews 344, 108962, http://doi.org/10.1016/j.quascirev.2024.108962

Gliganic, L.A., McDonald, J., Mather, C., White, L.T., 2024. A method to date rock engravings using luminescence – tested at Murujuga, Western Australia. Quaternary Geochronology 85, 101633, http://doi.org/10.1016/j.quageo.2024.101633

Gonzales-Lorenzo, C.D., Pacompia, Y., Cano, N.F., Rocca, R.R., Chubaci, J.F.D., Sullasi, H.S.L., Vilca, Z.V., Ayca-Gallegos, O., Ayala-Arenas, J., 2024. Quartz OSL dating of ancient ceramics fragments from the Churajon archaeological complex in Arequipa, Peru. Quaternary International 707, 38-49, http://doi.org/10.1016/j.quaint.2024.07.008

Härtling, J.W., Stele, A., Ortisi, S., Jepsen, A., Rappe, M., Bussmann, J., Fülling, A., 2025. Germanic Rampart or Roman Encampment?—New Geoarchaeological Evidence at the Roman Conflict Site at Kalkriese (NW-Germany). Geoarchaeology 40, e22031, http://doi.org/10.1002/gea.22031

Jin, J., Wei, J., Ling, Z., Hou, C., Xu, D., Li, Z., 2025. Optically dating of a Paleolithic site in coastal regions of South China and its correlation with the late Pleistocene environment evolution. Journal of Archaeological Science: Reports 61, 104887, http://doi.org/10.1016/j.jasrep.2024.104887

Karimi Moayed, N., Vandenberghe, D., Deforce, K., Kaptijn, E., Lambers, K., Verschoof-van der Vaart, W., De Clercq, W., De Grave, J., 2024. Optical dating of charcoal kiln remains from WWII: A test of accuracy. Quaternary Geochronology 83, 101582, http://doi.org/10.1016/j.quageo.2024.101582

Lambard, J.-B., Pereira, A., Voinchet, P., Guillou, H., Reyes, M.C., Nomade, S., Gallet, X., Belarmino, M., Bahain, J.-J., De Vos, J., Falguères, C., Cosalan, A., Ingicco, T., 2024. Geochronological advances in human and proboscideans first arrival date in the Philippines archipelago (Cagayan valley, Luzon Island). Quaternary Geochronology 84, 101597, http://doi.org/10.1016/j.quageo.2024.101597

MacDonald, B.L., Velliky, E.C., Forrester, B., Riedesel, S., Linstädter, J., Kuo, A.L., Woodborne, S., Mabuza, A., Bader, G.D., 2024. Ochre communities of practice in Stone Age Eswatini. Nature Communications 15, 9201, http://doi.org/10.1038/s41467-024-53050-6

Martínez-Pillado, V., Demuro, M., Ortiz, J.E., Shao, Q., Arnold, L.J., Duval, M., Cheng, H., Torres, T., Santos, E., Falguères, C., Tombret, O., García, N., Aranburu, A., Gómez-Olivencia, A., Arsuaga, J.L., 2024. Constraining the age of the Pleistocene sedimentary infill of Cueva Mayor (Atapuerca, N Spain) through a multi-technique dating approach. Quaternary Geochronology 83, 101576, http://doi.org/10.1016/j.quageo.2024.101576

Ponomareva, I.A., Hatte, L., Kemp, J., Wallace, M., McLennan, C., 2024. The archaeology of sacred womens' business in Australia: a Holocene history from the Central Queensland Highlands. Archaeology in Oceania 59, 333-349, http://doi.org/10.1002/arco.5328

Richard, M., Mercier, N., Weinstein-Evron, M., Weissbrod, L., Shimelmitz, R., 2024. Chronology of the late Lower and Middle Palaeolithic at Tabun Cave (Mount Carmel, Israel) with insights into diagenesis and dose rate variation using post-IR IRSL (pIRIR290) dating and infrared spectroscopy. Quaternary Geochronology 84, 101611, http://doi.org/10.1016/j.quageo.2024.101611

Sala, N., Alcaraz-Castaño, M., Arriolabengoa, M., Martínez-Pillado, V., Pantoja-Pérez, A., Rodríguez-Hidalgo, A., Téllez, E., Cubas, M., Castillo, S., Arnold, L.J., Demuro, M., Duval, M., Arteaga-Brieba, A., Llamazares, J., Ochando, J., Cuenca-Bescós, G., Marín-Arroyo, A.B., Seijo, M.M., Luque, L., Alonso-Llamazares, C., Arlegi, M., Rodríguez-Almagro, M., Calvo-Simal, C., Izquierdo, B., Cuartero, F., Torres-Iglesias, L., Agudo-Pérez, L., Arribas, A., Carrión, J.S., Magri, D., Zhao, J.X., Pablos, A., Nobody's land? The oldest evidence of early Upper Paleolithic settlements in inland Iberia. Science Advances 10, eado3807, http://doi.org/10.1126/sciadv.ado3807

Saleh, M., Polymeris, G.S., Panzeri, L., Tsoutsoumanos, E., Ricci, G., Secco, M., Martini, M., Artioli, G., Dilaria, S., Galli, A., 2024. Analysis probes and statistical parameters affecting the OSL ages of mortar samples; a case study from Italy. Radiation Physics and Chemistry 214, 111298, http://doi.org/10.1016/j.radphyschem.2023.111298

Samper Carro, S.C., Vega Bolivar, S., Pizarro Barbera, J., Westbury, E., Connor, S., Allué, E., Benito-Calvo, A., Arnold, L.J., Demuro, M., Price, G.J., Martinez-Moreno, J., Mora, R., 2024. Living on the edge: Abric Pizarro, a MIS 4 Neanderthal site in the lowermost foothills of the southeastern Pre-Pyrenees (Lleida, Iberian Peninsula). Journal of Archaeological Science 169, 106038, http://doi.org/10.1016/j.jas.2024.106038

Shipton, C., Morley, M.W., Kealy, S., Norman, K., Boulanger, C., Hawkins, S., Litster, M., Withnell, C., O'Connor, S., 2024. Abrupt onset of intensive human occupation 44,000 years ago on the threshold of Sahul. Nature Communications 15, 4193, http://doi.org/10.1038/s41467-024-48395-x

Slack, M.J., Law, W.B., Coster, A.C.F., Ditchfield, K., Field, J., Garvey, J., Gliganic, L.A., Moss, P., Paul, J.W., Reynen, W., Ward, I., Wasef, S., 2024. A 47,000 year archaeological and palaeoenvironmental record from Juukan 2 rockshelter on the western Hamersley Plateau of the Pilbara region, Western Australia. Quaternary Science Reviews 338, 108823, http://doi.org/10.1016/j.quascirev.2024.108823

Stewart, M., Andrieux, E., Blinkhorn, J., Guagnin, M., Fernandes, R., Vanwezer, N., Hatton, A., Alqahtani, M., Zalmout, I., Clark-Wilson, R., Al-Mufarreh, Y.S.A., Al-Shanti, M., Zahrani, B., Al Omari, A., Al-Jibreen, F., Alsharekh, A.M., Scerri, E.M.L., Boivin, N., Petraglia, M.D., Groucutt, H.S., 2024. First evidence for human occupation of a lava tube in Arabia: The archaeology of Umm Jirsan Cave and its surroundings, northern Saudi Arabia. PLOS ONE 19, e0299292, http://doi.org/10.1371/journal.pone.0299292

Taffin, N., Lahaye, C., Contreras, D.A., Holcomb, J.A., Mihailović, D.D., Karkanas, P., Guérin, G., Athanasoulis, D., Carter, T., 2024. Chronological and post-depositional insights from single-grain IRSL dating of a Palaeolithic sequence at Stelida, Naxos (Greece). Journal of Archaeological Science: Reports 59, 104776, http://doi.org/10.1016/j.jasrep.2024.104776

Taxel, I., Roskin, J., Grono, E., Balila, M., Bookman, R., Ostrowski, A., Shor, M., Asscher, Y., Porat, N., Robins, L., 2023. Limekiln services soil enrichment and water retention of an Early Islamic Plot-and-Berm groundwater-harvesting agroecosystem in coastal dunes near Caesarea, Israel. Archaeological and Anthropological Sciences 15, 170, http://doi.org/10.1007/s12520-023-01875-5

Wang, F.-G., Yang, S.-X., Ge, J.-Y., Ollé, A., Zhao, K.-L., Yue, J.-P., Rosso, D.E., Douka, K., Guan, Y., Li, W.-Y., Yang, H.-Y., Liu, L.-Q., Xie, F., Guo, Z.-T., Zhu, R.-X., Deng, C.-L., d'Errico, F., Petraglia, M., 2022. Innovative ochre processing and tool use in China 40,000 years ago. Nature 603, 284-289, http://doi.org/10.1038/s41586-022-04445-2

Wei, J., Jin, J., Fu, L., Zuo, X., Qiu, J., Hou, C., Xu, D., 2024. New chronology evidence of prehistoric human activities indicated by pottery luminescence dating in the humid subtropical mountains of South China. Journal of Archaeological Science 171, 106072, http://doi.org/10.1016/j.jas.2024.106072

ESR, applied in various contexts

Arnold, L.J., Demuro, M., Duval, M., Grün, R., Sanz, M., Costa, A.M., Araújo, A.C., Daura, J., 2024. Single-grain luminescence and combined U-series/ESR dating of the early Upper Palaeolithic Lagar Velho Rock Shelter, Leiria, Portugal. Quaternary Geochronology 83, 101572, http://doi.org/10.1016/j.quageo.2024.101572

Bartz, M., Duval, M., Alonso Escarza, M.J., Rixhon, G., 2024. Older than expected: fluvial aggradation of the Rhine's main terrace at Kärlich dated around 1.5 Ma by electron spin resonance. E&G Quaternary Science Journal 73, 139-144, http://doi.org/10.5194/egqsj-73-139-2024

Ben Arous, E., Bateman, M.D., Duval, M., 2024. Extending the ESR and OSL dating comparison on coastal dune deposits from the Wilderness-Knysna area (South Africa). Quaternary Geochronology 83, 101580, http://doi.org/10.1016/j.quageo.2024.101580

Ben Arous, E., Niang, K., Blinkhorn, J.A., Del Val, M., Medialdea, A., Coussot, C., Alonso Escarza, M.J., Bateman, M.D., Churruca Clemente, A., Blackwood, A.F., Iglesias-Cibanal, J., Saíz, C., Scerri, E.M.L., Duval, M., 2024. Constraining the age of the Middle Stone Age locality of Bargny (Senegal) through a combined OSL-ESR dating approach. Quaternary Environments and Humans 2, 100044, http://doi.org/10.1016/j.qeh.2024.100044

Benzid, K., Tani, A., 2024. Thermal behavior of E′ point defects in gamma-irradiated natural quartz: Study of the Meyer-Neldel rule using electron spin resonance. Journal of Luminescence 265, 120218, http://doi.org/10.1016/j.jlumin.2023.120218

Chourio-Camacho, D., Grimaud, J.-L., Tissoux, H., Bessin, P., Voinchet, P., Vartanian, E., Noble, M., Bertran, P., 2024. Incision and rock uplift along the Lower Seine River since Marine Isotope Stage 8. Journal of Quaternary Science 39, 872-889, http://doi.org/10.1002/jqs.3640

Demuro, M., Arnold, L.J., Duval, M., Churruca Clemente, A., Santonja, M., Pérez-González, A., 2024. Extended-range luminescence and ESR dating of Iberian fluvial terraces (Duero and Guadiana basins) associated with the Lower Palaeolithic sites of La Maya I, II, III, Burganes and Albalá (west-central Spain). Quaternary Geochronology 83, 101567, http://doi.org/10.1016/j.quageo.2024.101567

Hernando-Alonso, I., Moreno, D., Ortega, A.I., Benito-Calvo, A., Alonso, M.J., Campaña, I., Parés, J.M., Cáceres, I., García-Medrano, P., Carbonell, E., Bermúdez de Castro, J.M., 2024. ESR chronology of the endokarstic deposits of Galería complex (Sierra de Atapuerca, Spain). Quaternary Geochronology 83, 101575, http://doi.org/10.1016/j.quageo.2024.101575

Ji, H., Liu, C.-R., Li, W.-P., Wei, C.-Y., Neupane, B., Yin, G.-M., 2024. Evaluating signal bleaching of Al and Ti–Li centers in fluvio-lacustrine sediments of Datong, North China, and its implications for the volcanic eruption chronology. Quaternary Geochronology 83, 101568, http://doi.org/10.1016/j.quageo.2024.101568

Lambard, J.-B., Pereira, A., Voinchet, P., Guillou, H., Reyes, M.C., Nomade, S., Gallet, X., Belarmino, M., Bahain, J.-J., De Vos, J., Falguères, C., Cosalan, A., Ingicco, T., 2024. Geochronological advances in human and proboscideans first arrival date in the Philippines archipelago (Cagayan valley, Luzon Island). Quaternary Geochronology 84, 101597, http://doi.org/10.1016/j.quageo.2024.101597

Martínez-Pillado, V., Demuro, M., Ortiz, J.E., Shao, Q., Arnold, L.J., Duval, M., Cheng, H., Torres, T., Santos, E., Falguères, C., Tombret, O., García, N., Aranburu, A., Gómez-Olivencia, A., Arsuaga, J.L., 2024. Constraining the age of the Pleistocene sedimentary infill of Cueva Mayor (Atapuerca, N Spain) through a multi-technique dating approach. Quaternary Geochronology 83, 101576, http://doi.org/10.1016/j.quageo.2024.101576

Obata, N., Toyoda, S., 2025. Thermal stability of the bleachable and unbleachable components of the ESR signals in sedimentary quartz. Radiation Measurements 180, 107327, http://doi.org/10.1016/j.radmeas.2024.107327

Prado, J.L., Duval, M., Demuro, M., Santos-Arévalo, F.J., Alberdi, M.T., Tomassini, R.L., Montalvo, C.I., Bonini, R., Favier-Dubois, C.M., Burrough, S., Bajkan, S., Gasparini, G.M., Bellinzoni, J., Fernández, F.J., García-Morato, S., Marin-Monfort, M.D., Adams, S., Zhao, J.-x., Beilinson, E., Fernández-Jalvo,

Y., 2024. Refining the chronology of Middle/Late Pleistocene fossil assemblages in the Argentine Pampas. Quaternary Science Reviews 344, 108958, http://doi.org/10.1016/j.quascirev.2024.108958
Sala, N., Alcaraz-Castaño, M., Arriolabengoa, M., Martínez-Pillado, V., Pantoja-Pérez, A., Rodríguez-Hidalgo, A., Téllez, E., Cubas, M., Castillo, S., Arnold, L.J., Demuro, M., Duval, M., Arteaga-Brieba, A., Llamazares, J., Ochando, J., Cuenca-Bescós, G., Marín-Arroyo, A.B., Seijo, M.M., Luque, L., Alonso-Llamazares, C., Arlegi, M., Rodríguez-Almagro, M., Calvo-Simal, C., Izquierdo, B., Cuartero, F., Torres-Iglesias, L., Agudo-Pérez, L., Arribas, A., Carrión, J.S., Magri, D., Zhao, J.X., Pablos, A., 2024. Nobody's land? The oldest evidence of early Upper Paleolithic settlements in inland Iberia. Science Advances 10, eado3807, http://doi.org/10.1126/sciadv.ado3807
Xu, X., Wei, C., Yin, G., Ji, H., Liu, C., Zhao, L., Yang, H., Yang, G., 2024. Application of multiple-centers ESR dating to middle Pleistocene fluviolacustrine sediments and insights into the dose underestimation from the Ti–H center at high equivalent doses. Quaternary Geochronology 85, 101635, http://doi.org/10.1016/j.quageo.2024.101635

Basic research

Baumgarten, F.H., Thomsen, K.J., Guérin, G., Buylaert, J.-P., Murray, A.S., 2024. Testing the accuracy of single-grain OSL dating on Eemian quartz samples. Quaternary Geochronology 84, 101602, http://doi.org/10.1016/j.quageo.2024.101602
Benzid, K., Tani, A., 2024. Thermal behavior of E′ point defects in gamma-irradiated natural quartz: Study of the Meyer-Neldel rule using electron spin resonance. Journal of Luminescence 265, 120218, http://doi.org/10.1016/j.jlumin.2023.120218
Bouscary, C., King, G.E., 2024. Exploring the use of averaged thermal kinetic parameters in luminescence thermochronometry. Radiation Measurements 176, 107215, http://doi.org/10.1016/j.radmeas.2024.107215
Choi, J., Chamberlain, E., Wallinga, J., 2024. Variance in pIRIR signal bleaching for single grains of feldspar. Quaternary Geochronology 83, 101577, http://doi.org/10.1016/j.quageo.2024.101577
Durcan, J.A., Duller, G.A.T., 2024. Further investigation of spatially resolved single grain quartz OSL and TL signals. Radiation Measurements 177, 107260, http://doi.org/10.1016/j.radmeas.2024.107260
Ferreira, N.M., Nunes, M.C.d.S., Yoshimura, E.M., Trindade, N.M., Chithambo, M.L., 2024. Luminescência opticamente estimulada em pastilhas de quartzo utilizando iluminação azul e verde. Brazilian Journal of Radiation Sciences 12, e2568, http://doi.org/10.15392/2319-0612.2024.2568
Huang, C., Li, S.-H., 2024. Photoluminescence studies of different types of feldspars and the implications to the dating application using a Raman system. Radiation Measurements 177, 107248, http://doi.org/10.1016/j.radmeas.2024.107248
Karsu Asal, E.C., 2023. Luminescent properties of natural amazonite from Pakistan. Journal of Radioanalytical and Nuclear Chemistry 332, 2401-2408, http://doi.org/10.1007/s10967-023-08911-7
Kumar, R., Kook, M., Jain, M., 2022. Does hole instability cause anomalous fading of luminescence in feldspar? Journal of Luminescence 252, 119403, http://doi.org/10.1016/j.jlumin.2022.119403
Li, D., Zhao, H., Xie, H., Khormali, F., Sun, A., Zhang, S., 2024. Influence of Na-feldspar grains within the K-feldspar fraction on sediments IRSL dating. Quaternary International 698, 49-58, http://doi.org/10.1016/j.quaint.2024.06.009
Mrozik, A., Bilski, P., Mandowski, A., Kłosowski, M., Budzanowski, M., Drop, J., Swakoń, J., Discher, M., 2024. Searching for TL/OSL dose rate effects in various luminescent materials. Radiation Measurements 176, 107211, http://doi.org/10.1016/j.radmeas.2024.107211
Niyonzima, P., Oehler, S., King, G.E., Schmidt, C., 2024. Investigating thermoluminescence signal saturation in quartz and feldspar using emission spectrometry. Radiation Measurements 177, 107262, http://doi.org/10.1016/j.radmeas.2024.107262
Obata, N., Toyoda, S., 2025. Thermal stability of the bleachable and unbleachable components of the ESR signals in sedimentary quartz. Radiation Measurements 180, 107327, http://doi.org/10.1016/j.radmeas.2024.107327
Ortiz, C., Parra, M., Rodrigues, F.C.G., Mineli, T.D., Sawakuchi, A.O., 2024. Tracing uplift and erosion in orogenic settings using quartz luminescence sensitivity: Insights from the Northern Andes uplift. Quaternary Geochronology 83, 101581, http://doi.org/10.1016/j.quageo.2024.101581
Rhodes, E.J., Spano, T.M.C., Hodge, R.A., Sawakuchi, A.O., Bertassoli, D.J., 2024. Single grain K-feldspar MET-IRSL sediment transport determination: Bleaching patterns and rates. Quaternary Geochronology 85, 101626, http://doi.org/10.1016/j.quageo.2024.101626
Singhal, M., Panda, M., Shinde, S.H., Mondal, S., Annalakshmi, O., Chauhan, N., 2024. Study of thermoluminescence characteristics of quartz for high radiation doses (>1kGy): Implications for

extending the luminescence dating range. Radiation Measurements 178, 107300, http://doi.org/10.1016/j.radmeas.2024.107300

Souza, P.E., Porat, N., Sawakuchi, A.O., Cruz, C.B.L., Breda, C., Rodrigues, F.C.G., Oliveira, S.C., Pupim, F.N., 2024. Using quartz OSL signals from SAR cycles for sediment provenance studies. Quaternary Geochronology 83, 101574, http://doi.org/10.1016/j.quageo.2024.101574

Tanski, N.M., Rittenour, T.M., Pavano, F., Pazzaglia, F., Mills, J., Corbett, L.B., Bierman, P., 2024. Quartz luminescence sensitivity enhanced by residence time in the critical zone. Quaternary Geochronology 84, 101613, http://doi.org/10.1016/j.quageo.2024.101613

Winzar, J.A., Duller, G.A.T., Roberts, H.M., Gunn, M., Bell, A.M.T., 2025. Intensity and optical resetting of Infrared Photoluminescence (IRPL) and Infrared Stimulated Luminescence (IRSL) signals in feldspars. Journal of Luminescence 278, 121018, http://doi.org/10.1016/j.jlumin.2024.121018

Dosimetry

Chumak, V., Bakhanova, E., Karampiperi, M., Bernhardsson, C., 2024. OSL dosimetry with table salt for mass screening of individual doses during radiological or nuclear emergencies. Radiation Measurements 177, 107233, http://doi.org/10.1016/j.radmeas.2024.107233

Motta, S., Yukihara, E.G., 2024. Assessing dose rate effects in TL and OSL dosimeters: A critical look into dose rate models. Radiation Measurements 179, 107305, http://doi.org/10.1016/j.radmeas.2024.107305

Mrozik, A., Kuźnik, D., Bilski, P., Discher, M., 2024. Investigating luminescence signals of pharmaceuticals and dietary supplements for emergency dosimetry. Radiation Measurements 177, 107225, http://doi.org/10.1016/j.radmeas.2024.107225

Instruments

Andričević, P., Kook, M., Jain, M., 2024. Potential of luminescence imaging for screening sensitive and well-bleached samples for rock surface luminescence dating. Radiation Measurements 176, 107193, http://doi.org/10.1016/j.radmeas.2024.107193

Dombrowski, H., Stenger, J., 2024. Energy calibration of LaBr3 detectors using inherent radioactivity. Journal of Instrumentation 19, P09033, http://doi.org/10.1088/1748-0221/19/09/P09033

Portable instruments

Bar, A., Zviely, D., Roskin, J., Galili, E., Porat, N., Bookman, R., 2024. Beachrock: A chronological benchmark for Late Holocene build-up on the coast of Israel. Geomorphology 465, 109408, http://doi.org/10.1016/j.geomorph.2024.109408

Euzen, C., Chabaux, F., Rixhon, G., Preusser, F., Eyrolle, F., Chardon, V., Zander, A.M., Badariotti, D., Schmitt, L., 2024. Multi-method geochronological approach to reconstruct post-1800 floodplain sedimentation in the upper Rhine plain, France. Quaternary Geochronology 83, 101561, http://doi.org/10.1016/j.quageo.2024.101561

Staff, R.A., Sanderson, D.C.W., Rex, C.L., Cresswell, A., Hyodo, M., Kitaba, I., Marshall, M.H., Schlolaut, G., Yamada, K., Suzuki, Y., Nowinski, V., Tada, R., Nakagawa, T., 2024. A luminescence-derived cryptostratigraphy from the Lake Suigetsu sedimentary profile, Japan: 45,000–30,200 IntCal20 yr BP. Quaternary Geochronology 83, 101588, http://doi.org/10.1016/j.quageo.2024.101588

Review

Chithambo, M., 2024. Phototransferred Thermoluminescence. IOP Publishing London. http://doi.org/ 10.1088/978-0-7503-3831-8

McKeever, S.W.S., 2024. A review of the optically and thermally stimulated luminescence properties of aluminosilicates. Optical Materials: X 24, 100351, http://doi.org/10.1016/j.omx.2024.100351

Statistics, simulation, and modelling

Chen, R., Lawless, J.L., Arora, R., 2024. Non-monotonic dose dependence of thermoluminescence (TL) revisited. Radiation Measurements 177, 107235, http://doi.org/10.1016/j.radmeas.2024.107235

Kitis, G., Pagonis, V., 2023. On the Need for Deconvolution Analysis of Experimental and Simulated Thermoluminescence Glow Curves. Materials 16, 871, http://doi.org/10.3390/ma16020871

Motta, S., Yukihara, E.G., 2024. Assessing dose rate effects in TL and OSL dosimeters: A critical look into dose rate models. Radiation Measurements 179, 107305, http://doi.org/10.1016/j.radmeas.2024.107305

Sørensen, A.L., Hansen, T.M., Nørgaard, J., Buylaert, J.-P., Murray, A.S., Kulakova, E., Kurbanov, R., Knudsen, M.F., 2024. CosmoChron: A versatile age-depth modeling approach using cosmogenic nuclides and direct age constraints. Quaternary Geochronology 85, 101618, http://doi.org/10.1016/j.quageo.2024.101618

Computer coding

Pagonis, V., 2022. Luminescence Signal Analysis Using Python. Springer Cham, http://doi.org/10.1007/978-3-030-96798-7

Conference Announcements: UKLum 2025

We are excited to announce the 2025 UK Luminescence and Electron Spin Resonance Dating Meeting, taking place in the beautiful town of St Andrews, Scotland from August 20-22, 2025. This informal gathering will serve as a platform to discuss the latest advancements and ongoing research in luminescence and ESR dating, with a particular focus on recent developments, ongoing projects, and student-led work. We encourage both oral and poster presentations, especially from students and early-career researchers.

To register your interest in attending the meeting and be added to the mailing list for future updates and circulars, please use this link: https://forms.office.com/e/SfJp8ZVw4S

Should you have any questions or need further information, don't hesitate to reach out to us at the conference-specific email address: ukled2025@st-andrews.ac.uk.

Stay tuned for more details on registration and the agenda. Mark your calendars—we can't wait to welcome you to Scotland!

Aayush Srivastava, Adrian Finch, Tim Kinnaird (St Andrews) and David Sanderson (SUERC)

Ancient TL

ISSN 2693-0935

Aims and Scope
Ancient TL is a journal devoted to Luminescence dating, Electron Spin Resonance (ESR) dating, and related techniques. It aims to publish papers dealing with experimental and theoretical results in this field, with a minimum of delay between submission and publication. Ancient TL also publishes a current bibliography, thesis abstracts, letters, and miscellaneous information, e.g., announcements for meetings.

Frequency
Two issues per annum in June and December

Submission of articles to Ancient TL
Ancient TL has a reviewing system in which direct dialogue is encouraged between reviewers and authors. For instructions to authors and information on how to submit to Ancient TL, please visit the website at:
http://ancienttl.org/TOC1.htm

Journal Enquiries
For enquiries please contact the editor:
Christoph Schmidt, Institute of Earth Surface Dynamics, University of Lausanne, 1015 Lausanne, Switzerland, Tel: +41-21-692-3516 (christoph.schmidt@unil.ch)

Subscriptions to Ancient TL
Ancient TL Vol. 32, No. 2 December 2014 was the last issue to be published in print. Past and current issues are available for download free of charge from the Ancient TL website:
http://ancienttl.org/TOC4.htm